Phase response to arbitrary perturbations: Geometric insights and resetting surfaces

Kyoung H. Lee[1], Neil G. R. Broderick[2], Bernd Krauskopf[1] and Hinke M. Osinga[1]

[1] Department of Mathematics and Dodd–Walls Centre for Photonic and Quantum Technologies, University of Auckland, Private Bag 92019, Auckland 1142, New Zealand

[2] Department of Physics and Dodd–Walls Centre for Photonic and Quantum Technologies, University of Auckland, Private Bag 92019, Auckland 1142, New Zealand

May 2024

Abstract

Phase resetting is an experimental tool, originally from neuroscience, for the study of oscillatory systems. A phase reset measures the phase shift that occurs as points on the oscillator return to an underlying stable periodic orbit Γ after a specific perturbation. Such a perturbation is along a given unit direction $\boldsymbol{d}$ in phase space with amplitude A, and it is applied to all points of Γ, which are parametrised by their phases ϑ_{o} (with respect to a reference point). The classical Phase Transition curve (PTC) in the literature is the graph of the circle map from ϑ_{o} to the new phase ϑ_{n} for fixed $\boldsymbol{d}$ and A.

We take a global, geometric point of view and consider the map to the new phase ϑ_{n} in dependence not only on ϑ_{o}, but also on $\boldsymbol{d}$ and A. Its graph is a reset hypersurface that encodes all phase information for any possible perturbation. Specifically, we study phase resets of a planar system in this way, where the direction $\boldsymbol{d}$ is given by an angle φ_{d}. Any slice through the reset hypersurface for fixed A is a reset surface in a three-torus that relates ϑ_{o}, φ_{d} and ϑ_{n}. We study what this surface looks like and how it changes topologically at isolated points of A; the latter involves the creation of singularities due to interactions with the phaseless set.

We explain and illustrate our findings with two example systems. First, we present a detailed case study of a constructed planar vector field designed by Winfree. It has the special and exceptional property that its isochrons (curves of given phase response) and, hence, the phase response can be computed analytically; in particular, the system is invariant under rotation about the origin. This allows us to study changes of the phase response in considerable detail. Our second example is the planar Van der Pol oscillator, which does not have the above special properties. Indeed, its isochrons and phase response are not known analytically and need to be computed numerically. We present a boundary value problem setup to find reset surfaces and study their properties in an efficient and effective way. This demonstrates that our global approach is computationally feasible for gaining insights into the geometry of phase responses of general (planar) oscillatory systems.

1 Introduction

Phase resetting is a widely adopted approach for evaluating neuronal responses in experiments: a spiking neuron is subjected to a current injection, which disrupts the regular spiking response and generally leads to a phase shift: the spike following the perturbation comes earlier or later than it would have occurred without the current injection; see [14, 25, 36, 37, 41] for experimental results. The nature of the phase shift depends on the magnitude of the current injection and its timing relative to the spiking activity.

The graph that relates the old phase to the resulting phase shift is called the *Phase Response Curve* (PRC). The PRC is particularly useful in the study of neuronal systems, as evidenced, for example, in [2, 11, 12, 21], and it can be used to distinguish between different types of neurons.

Hodgkin [22] introduced a classification that categorises neurons as Type I or Type II. A Type I neuron exhibits a PRC with a consistent sign, either positive or negative, while Type II neurons have PRCs that change sign; Type II neurons are also less likely to fire at low-frequency firing rates [11, 13].

Winfree [15, 47, 49] considered the graph that relates the old phase directly to the new phase, which he called the *Phase Transition Curve* (PTC). A phase reset is defined as type 1 (or weak) if the PTC increases or decreases by 1 when the old phase is varied over 1, and as type 0 (or strong) when there is no phase increase or decrease between ϑ_o and $\vartheta_\mathrm{o}+1$. Careful experiments with the yeast cycle and the hatching of fruit flies in [47] allowed Winfree to represent the measured phase response as a surface in the three-dimensional space of new phase over the plane of old phase and perturbation amplitude; his "resetting surface" is a helicoid with a vertical "singular axis", which distinguishes the PTCs of type 1 for smaller perturbation amplitudes from those of type 0 for larger ones. Mathematically, this difference can be interpreted in terms of which type of torus knot they form (as a graph on the torus of input versus output phase) [24, 29]; namely, a $1:1$ torus knot with winding number 1 for type 1, and a $1:0$ torus knot with winding number 0 for type 0. This topological difference is behind the proof of the conjecture by Winfree that the existence of a PTC of type 0 necessarily implies the existence of a singularity (at least one) where the PTC is discontinuous [24].

In the study of weakly coupled oscillators, PRCs or PTCs are useful for obtaining a so-called phase reduction. This requires that the respective curve is well approximated by the linearised system, meaning that, over a sufficiently large range of perturbation amplitudes, the it is very similar to the one resulting from an infinitesimally small perturbation. The technique of phase reduction transforms a potentially high-dimensional model of a single oscillator into a one-dimensional phase equation. For the study of networks of coupled oscillators, multiple phase equations are derived and coupled using phase reduction to analyse synchronisation [31, 39, 40]. However, experiments have revealed the limitations of standard phase reduction when dealing with complicated coupled oscillators [32, 45]. When the PRC or PTC is no longer well approximated by the linearised system, higher-order approximations are needed that take into account the dependence on the perturbation amplitude. Various such amplitude-phase reduction techniques have been developed to improve validity of the reduced model for larger ranges of perturbation amplitudes [3, 4, 30, 38, 46].

In this paper, we take a global, geometric approach that captures all possible phase resets of a given system. More specifically, we consider the phase response in dependence on the full range of perturbation amplitudes and, moreover, also as a function of any *direction* of the perturbation used in the phase reset. The basic setting is that of a dynamical system with an attracting periodic orbit; the perturbation is applied at a point along this periodic orbit, in any direction and with any amplitude, and we determine the new phase after relaxation back to the periodic attractor.

To be more precise, we consider systems of the form

$$\dot{\boldsymbol{x}} = \boldsymbol{F}(\boldsymbol{x}), \tag{1}$$

where $\boldsymbol{F}:\mathbb{R}^n\to\mathbb{R}^n$ is at least once continuously differentiable. We assume that there exists an attracting (and hyperbolic) periodic orbit

$$\Gamma := \{\gamma(t)\in\mathbb{R}^n \mid t\in\mathbb{R} \text{ with } \gamma(t)=\gamma(t+T_\Gamma)\},$$

where $\gamma(t)$ is a solution (or trajectory) of (1) and $T_\Gamma>0$ is the (minimal) period. Hence, γ is a covering map of Γ that is bijective for $t\in[0,T_\Gamma)$. As is the convention in the field, we assume that the first point $\gamma(0)=\gamma_0\in\Gamma$ lies at the maximum of the solution with respect to the first component. We define the phase $\vartheta\in\mathbb{S}^1$ for each point $\gamma(t)\in\Gamma$ as the fraction $\vartheta := t/T_\Gamma$ of the

period; note that, throughout, we parametrise the circle $\mathbb{S}^1$ by $\vartheta \in [0,1)$. Following Winfree [49], we assign a *latent phase* to any point $\boldsymbol{x}_0$ in the basin of attraction $\mathcal{B}(\Gamma)$ of Γ, defined as the value $\vartheta \in \mathbb{S}^1$ such that the trajectory $\boldsymbol{x}(t)$ of (1) with $\boldsymbol{x}(0) = \boldsymbol{x}_0$ converges to Γ in phase with γ_ϑ; more precisely, for $K \in \mathbb{N}$, we have

$$\lim_{K\to\infty} \|\boldsymbol{x}(K\,T_\Gamma) - \gamma_\vartheta\| = 0.$$

Winfree already observed that any point $\boldsymbol{x}_0 \in \mathcal{B}(\Gamma)$ has a unique latent phase and he defined the set I_ϑ of points with the same latent phase ϑ, which he called the *isochron* of γ_ϑ. Guckenheimer [16] showed that each isochron I_ϑ is an $(n-1)$-dimensional manifold that contains γ_ϑ. More precisely, I_ϑ is the stable manifold of the fixed point $\gamma_\vartheta \in \Gamma$ under the time-T_Γ map, and the family $\mathcal{I} := \{I_\vartheta\}_{\vartheta\in\mathbb{S}^1}$ of all isochrons foliates the basin $\mathcal{B}(\Gamma)$.

Geometrically, the reset of a point $\gamma_{\vartheta_\mathrm{o}} \in \Gamma$ with (old) phase $\vartheta = \vartheta_\mathrm{o}$ that is perturbed to a point $\boldsymbol{x}_0 \in \mathcal{B}(\Gamma)$ is given by the unique (new) phase ϑ_n for which $\boldsymbol{x} \in I_{\vartheta_\mathrm{n}}$. Any perturbation is given by a unit direction vector $\boldsymbol{d} \in \mathbb{S}^{n-1} \subset \mathbb{R}^n$ together with a positive amplitude $A \in \mathbb{R}_0^+$, where $\mathbb{S}^{n-1}$ is the $(n-1)$- dimensional sphere. Hence, the above requirement is that $\boldsymbol{x}_0 = \gamma_{\vartheta_\mathrm{o}} + A\,\boldsymbol{d} \in \mathcal{B}(\Gamma)$ for the chosen $\boldsymbol{d}$ and A. If this is not the case then the reset is not defined, and this is why the complement of $\mathcal{B}(\Gamma)$ is also called the *phaseless set*. Winfree observed that the basin boundary $\partial\mathcal{B}(\Gamma) = \overline{\mathcal{B}(\Gamma)} \setminus \mathcal{B}(\Gamma)$ has the property that all isochrons in the family $\mathcal{I}$ intersect any neighbourhood (no matter how small) of a point in $\partial\mathcal{B}(\Gamma)$ [16, 48]. Consequently, resets near $\partial\mathcal{B}(\Gamma)$ lead to large phase sensitivity.

The 'traditional view' to phase resetting is to fix the direction vector $\boldsymbol{d}$ and consider the PRC or PTC for different values of the perturbation amplitude A, so that the difference between the above mentioned types can be investigated [15, 47, 49]. However, one might also ask how the phase after perturbation depends on the direction vector $\boldsymbol{d}$ for fixed A, or on any combination of A and $\boldsymbol{d}$ of interest. This motivates us to take the more global and quite natural point of view of considering simultaneously the dependence of ϑ_n on *all aspects of the perturbation*: where it is applied along Γ, its direction $\boldsymbol{d}$ and amplitude A. In other words, for an attracting periodic orbit in $\mathbb{R}^n$, we consider the resetting map

$$\begin{array}{rccccc} \mathcal{P} & : & \mathbb{S}^1 \times \mathbb{S}^{n-1} \times \mathbb{R}_0^+ & \to & \mathbb{S}^1 \\ & & (\vartheta_\mathrm{o}, \quad \boldsymbol{d}, \quad A) & \mapsto & \vartheta_\mathrm{n}, \end{array} \tag{2}$$

defined by the property that

$$\gamma_{\vartheta_\mathrm{o}} + A\,\boldsymbol{d} \in I_{\vartheta_\mathrm{n}}. \tag{3}$$

In practice, one needs to choose a parametrisation of $\boldsymbol{d} \in \mathbb{S}^{n-1} \subset \mathbb{R}^n$ by $n-1$ angles.

We refer to the graph of $\mathcal{P} \subset \mathbb{S}^1 \times \mathbb{S}^{n-1} \times \mathbb{R}_0^+ \times \mathbb{S}^1$ as the *resetting hypersurface*, and it encodes all resetting information. Since it is of dimension at least 3, we find it useful to consider two-dimensional 'slices' of graph($\mathcal{P}$) in selected three-dimensional subspaces; this is achieved by fixing A or ϑ_o and/or (a sufficent number of) angles parametrising $\boldsymbol{d}$ in a particular way. We refer to the associated slice of graph($\mathcal{P}$) as a *resetting surface*; indeed, the helical resetting surface Winfree drew in [47, Fig. 4] is an example of a slice for fixed $\boldsymbol{d}$.

We will demonstrate this geometric point of view with two planar systems, where $n = 2$ and $\boldsymbol{d}$ is given by a single angle φ_d. Here, the two-dimensional intersection of graph($\mathcal{P}$) with the subspace of fixed φ_d captures the entire transition of the PTC from type 1 to type 0. Alternatively fixing ϑ_o, that is, the point of Γ where the perturbation is applied, provides a complementary and dual view of how the resetting depends on the direction $\boldsymbol{d}$. As we will show in subsequent sections, resetting surfaces for a sequence of fixed values of the amplitude A, which we refer to as graph($\mathcal{P}_A$), provide insight into geometric and topological changes of the overall phase resetting. In particular, we show that there is a one-to-one correspondence between the geometry of the isochron foliation near the phaseless set and that of resetting surfaces near

their singularities. Our findings extend and bring the mathematical viewpoint full circle with Winfree's interpretation of his experimental data.

This paper proceeds as follows. In Sec. 2, we introduce Winfree's model and subsequently use it to investigate the properties of graph($\mathcal{P}$) in detail. This planar vector field has rotational symmetry: its attracting periodic orbit is the unit circle and the origin is a repellor and the only point in the phaseless set. Moreover, the function $\mathcal{P}$ can be studied analytically because the isochrons of the system are known analytically as parametrised curves; in fact, depending on the value of a parameter they are straight lines or they spiral into the origin. These special properties make Winfree's model an good test-case example for our purposes. We first consider the case of straight isochrons and recall in Sec. 2.1 the notions of PRC and PTC and how they change type with A; here, we also introduce the dual *Directional Transition Curve* (DTC), which describes the resetting as a function of φ_d for fixed ϑ_o and A. Specifically, we illustrate how the intersection of the respective *perturbation set* for fixed A, consisting of all perturbations (as a function of ϑ_o and φ_d, respectively), determines the nature of the PTC and of the DTC. Section 2.2 then discusses and explains the associated transitions of the PTC and the DTC in terms of resetting surfaces, including their singularities that arise due to the respective perturbed point being exactly the origin (the phaseless set).

We then turn to the case that the isochrons in Winfree's model spiral around the phaseless set, which is the generic situation. This introduces an additional complexity in the transition from type 1 to type 0 of the PTCs that has not been discussed before, and similarly for the DTC. We discuss in Sec. 2.3 what this transition looks like at the level of these curves, and then present in Sec. 2.4 the corresponding resetting surfaces and their associated singularities. Due to the spiralling of the isochrons, the transition between torus-knot type is quite dramatic and involves the accumulation of the PTC or DTC on a circle; this implies that the image ϑ_n is covered more and more, inifinitely many times at the singularity, and then less and less. We explain this process in Sec. 2.5 by sequences of what we call *twin tangencies* between isochrons and the perturbation set, as the latter moves over the origin with A. This is a generic phenomenon when the isochrons are spirals around an equilibrium of a planar system.

Due to its rotational symmetry, Winfree's model is not representative when it comes to the structure of graph($\mathcal{P}_A$) and its geometric and topological changes with A. Firstly, the function $\mathcal{P}$ is generally not known analytically, and resetting surfaces of interest must be found numerically. We demonstrate in Sec. 3 with the example of the planar Van der Pol system that this can be achieved by formulating and solving for solution families of a multi-segment boundary value problem (BVP). Our computational approach is based on that in [29] and implemented in the MATLAB-based software package COCO [5]; its key aspects are discussed briefly in Appendix A. Secondly, the attracting periodic orbit in Winfree's model is a perfect circle with the phaseless set at its centre; hence, all points on the periodic orbit have the same distance to the phaseless set. This is generically not the case, and we show in Sec. 3.1 what this means for the PTCs and DTCs of the Van der Pol system. The geometry of the accociated resetting surface graph($\mathcal{P}_A$) for increasing A is then presented in Sec. 3.2; Notably, singularities of it now occur over a range of A (rather than only for $A = 1$ as in Winfree's model): they are created and disappear when A is the minimal and maximal distance of any point Γ to the origin, which is again the phaseless set here. Sequences of twin tangencies of the DTC occur in the Van der Pol system as well. However, as Sec. 3.3 shows, their A-values are extremely close to that of the transtion from a $1:0$ to a $1:1$ torus knot, which is due to the isochrons being very steep spirals.

In the final Sec. 4, we draw some general conclusions and point out how our approach can be used more widely to understand qualitative changes in phase resetting arising from transitions through more complicated phaseless sets, such as those studied in [19] in the context of planar systems.

2 Case study of resetting in Winfree's model

In the 1970s, Winfree constructed several planar oscillator models that were sufficiently simple for him to find explicit expressions of their isochrons; see [48] and Examples 1–4 in the chapter *Attracting Cycles and Isochrons* in [49]. In the same spirit, we combine his Examples 2 and 4 into the following system, defined in polar coordinates $(R, \phi) \in \mathbb{R}_0^+ \times \mathbb{S}^1$ as

$$\begin{cases} \dot{R} &= \kappa\,(1-R)R^2, \\ \dot{\phi} &= 1+\varepsilon(1-R). \end{cases} \tag{4}$$

Winfree used the fixed values $\kappa = 5$ in Example 2 and $\kappa = 1$ in Example 4.

Note that the right-hand sides of both equations only depend on the radial component R. Consequently, the flow is invariant under any translation in ϕ, and the equation for R identifies the trajectory with $R = 1$ as the only attracting solution. This means that the unit circle in the plane of Euclidean coordinates is an attracting periodic orbit Γ whose basin is the entire plane except for the origin $\mathbf{0}$. Winfree takes derivatives with respect to scaled time in units of the period of this periodic orbit; hence, the period of Γ is 1.

Translation invariance is the property that makes it possible to find an explicit formulation for the isochrons. In complete analogy to Winfree's derivation from [49], the isochrons are given by the level sets of the function

$$\Phi(R,\phi) = \phi + \frac{\varepsilon}{\kappa\,R} - \frac{\varepsilon}{\kappa}. \tag{5}$$

Hence, I_ϑ is defined implicitly as the level set $\Phi(R,\phi) = \vartheta$, which for each $\vartheta \in \mathbb{S}^1$ can be formulated explicitly as the R-parametrised curve

$$I_\vartheta := \left\{ (R,\phi(R)) \in \mathbb{R}_0^+ \times \mathbb{S}^1 \;\middle|\; \phi(R) = \vartheta + \tfrac{\varepsilon}{\kappa} - \tfrac{\varepsilon}{\kappa R} \right\}. \tag{6}$$

We consider system (4) as a system in Euclidean coordinates, given by $x = R\cos(2\pi\,\phi)$ and $y = R\sin(2\pi\,\phi)$, and we fix $\kappa = 2\pi$ thoughout. This the convenient choice leads to the system

$$\begin{cases} x' &= -(1+\varepsilon)\,y + (x+\varepsilon\,y)\sqrt{x^2+y^2} - x(x^2+y^2), \\ y' &= (1+\varepsilon)\,x - (\varepsilon\,x - y)\sqrt{x^2+y^2} - y(x^2+y^2), \end{cases} \tag{7}$$

where the derivative is now taken with respect to the 'standard' time where Γ has period 2π. The origin $\mathbf{0}$ is the only equilibrium; it is a repelling focus (with complex conjugate eigenvalues) and the only point in the phaseless set. The translation invariance of system (4) is equivalent to invariance of (7) under any rotation of the (x,y)-plane about $\mathbf{0}$; in particular, for any $\vartheta \in \mathbb{S}^1$ the isochron I_ϑ is given in Euclidean coordinates by $x = R\cos(2\pi\,\phi)$ and $y = R\sin(2\pi\,\phi)$, with $\phi = \phi(R)$ as defined in (6).

Recall that the resetting map $\mathcal{P}$ for $n = 2$ with $(\vartheta_\mathrm{o}, \varphi_\mathrm{d}, A) \in \mathbb{S}^1 \times \mathbb{S}^{n-1} \times \mathbb{R}_0^+$ is defined as the unique latent phase ϑ_n such that $\gamma(\vartheta_\mathrm{o}) + A\,\boldsymbol{d}(\varphi_\mathrm{d}) \in I_{\vartheta_\mathrm{n}}$. For Winfree's model in the form of system (7), the explicit expression for I_ϑ via (6) allows us to find an implicit equation that relates triples $(\vartheta_\mathrm{o}, \varphi_\mathrm{d}, A)$ with $\vartheta_\mathrm{n} \in \mathbb{S}^1$ and, hence, defines graph$(\mathcal{P})$. However, this fails when the triple $(\vartheta_\mathrm{o}, \varphi_\mathrm{d}, A)$ is such that $\gamma(\vartheta_\mathrm{o}) + A\,\boldsymbol{d}(\varphi_\mathrm{d}) = \mathbf{0}$, that is, this perturbation lies on the only point in the phaseless set; at such points, $\mathcal{P}(\vartheta_\mathrm{o}, \varphi_\mathrm{d}, A)$ is not defined and graph$(\mathcal{P})$ has a singularity.

2.1 PRC, PTC and DTC for straight-line isochrons

To introduce and discuss the properties of the PRC, the PTC and also the new DTC, we start off with the geometrically simplest and rather special case with $\varepsilon = 0$ when the flow of

system (7) has constant angular velocity in the anticlockwise direction. In particular, according to equation (6) all isochrons are then the straight rays from $\mathbf{0}$ given by

$$I_\vartheta := \left\{ (R, \phi(R)) \in \mathbb{R}_0^+ \times \mathbb{S}^1 \;\middle|\; \phi(R) = \vartheta \right\}.$$

Therefore, $\vartheta_\mathrm{n} = \mathcal{P}(\vartheta_\mathrm{o}, \varphi_\mathrm{d}, A)$ is defined as the latent phase of the point

$$\gamma(\vartheta_\mathrm{o}) + A\,\boldsymbol{d}(\varphi_\mathrm{d}) = \begin{bmatrix} \cos(2\pi\,\vartheta_\mathrm{o}) + A\,\cos(2\pi\,\varphi_\mathrm{d}) \\ \sin(2\pi\,\vartheta_\mathrm{o}) + A\,\sin(2\pi\,\varphi_\mathrm{d}) \end{bmatrix}.$$

In other words, we seek $\vartheta_\mathrm{n} \in \mathbb{S}^1$ such that

$$\begin{aligned} &\sin(2\pi\,\vartheta_\mathrm{n})\,(\cos(2\pi\,\vartheta_\mathrm{o}) + A\,\cos(2\pi\,\varphi_\mathrm{d})) \\ =\;& \cos(2\pi\,\vartheta_\mathrm{n})\,(\sin(2\pi\,\vartheta_\mathrm{o}) + A\,\sin(2\pi\,\varphi_\mathrm{d})), \end{aligned}$$

where we use the convention that no solution exists if $(\vartheta_\mathrm{o}, \varphi_\mathrm{d}, A)$ are such that the equality holds trivially, that is, when $\cos(2\pi\,\vartheta_\mathrm{o}) + A\,\cos(2\pi\,\varphi_\mathrm{d}) = \sin(2\pi\,\vartheta_\mathrm{o}) + A\,\sin(2\pi\,\varphi_\mathrm{d}) = 0$. Simplification with the trigonometric angle sum identity gives

$$\sin(2\pi\,(\vartheta_\mathrm{n} - \vartheta_\mathrm{o})) = -A\,\sin(2\pi\,(\vartheta_\mathrm{n} - \varphi_\mathrm{d})), \tag{8}$$

where again the convention is that no solution exists if $(\vartheta_\mathrm{o}, \varphi_\mathrm{d}, A)$ are such that this equality holds trivially for any $\vartheta_\mathrm{n} \in \mathbb{S}^1$.

The 'classical' PRC and the PTC are readily computed from the implicit equation (8), and Fig. 1 illustrates three different phase resets in the fixed direction $\boldsymbol{d} = [1, 0]$, that is, with $\varphi_\mathrm{d} = 0$, for perturbation amplitudes $A = 0.5$, $A = 1$, and $A = 1.5$. Panel (a) shows Γ and 20 isochrons uniformly distributed in phase. Also shown are the corresponding three shifted versions of Γ for these three values of A, which we refer to as *perturbation sets* defined by $\Gamma_A := \{\gamma_{\vartheta_\mathrm{o}} + A\,\boldsymbol{d} \mid \vartheta_\mathrm{o} \in \mathbb{S}^1\}$. The phase response is determined by how each perturbation set intersects the isochrons. Plotting the corresponding phase shifts $\Delta(\vartheta_\mathrm{o}) = \vartheta_\mathrm{n} - \vartheta_\mathrm{o}$ and new phases $\vartheta_\mathrm{n}(\vartheta_\mathrm{o})$ for all $\vartheta_\mathrm{o} \in [0, 1)$ gives the three PRCs and PTCs shown in Fig. 1(b) and (c), respectively. Note that the range for ϑ_n in panel (c) has been extended beyond $[0, 1)$ for illustrative purposes to show the periodic nature of the PTCs, which is the graph of the circle map from $\vartheta_\mathrm{o} \in \mathbb{S}^1$ to $\vartheta_\mathrm{n} \in \mathbb{S}^1$; here and in all similar figures, the shaded unit square $[0, 1) \times [0, 1)$ is the standard representation of the torus $\mathbb{S}^1 \times \mathbb{S}^1$ (its fundamental domain in the covering space $\mathbb{S}^1 \times \mathbb{S}^1$) on which this graph lives.

For the trivial case that $A = 0$ we have $\Gamma_0 = \Gamma$, which means that the PRC in Fig. 1(b) is the constant function 0. The associated PTC in Fig. 1(c) is the graph of the identity, which is of type 1 with winding number 1; mathematically, it forms a $1:1$ torus knot on the torus. For all $0 < A < 1$ the perturbation set Γ_A surrounds the phaseless set $\mathbf{0}$ and intersects all isochrons in the family $\mathcal{I}$; the shown case for $A = 0.5$ is representative for this interval of perturbation amplitudes. Since the isochrons are linear, the horizontal translations of γ_0 and $\gamma_{0.5}$ along $\boldsymbol{d}$ always lie on their respective isochrons I_0 and $I_{0.5}$. Consequently, $\Delta(0) = \Delta(0.5) = 0$ in Fig. 1(b), and these values are actually sign changes of the PRC, which is therefore of Type II. Notice further from equation (8) that the phase difference $\Delta(\vartheta_\mathrm{o}) = \vartheta_\mathrm{n} - \vartheta_\mathrm{o}$ ranges between $\pm\frac{1}{2\pi}\sin^{-1}(A)$ when $A \leq 1$. Similarly, for the PTC in Fig. 1(c) we have that $\vartheta_\mathrm{n} = \vartheta_\mathrm{o}$ when $\vartheta_\mathrm{o} = 0$ or $\vartheta_\mathrm{o} = 0.5$; moreover, the PTC is still a $1:1$ torus knot, and so remains of type 1.

When $A > 1$, the perturbation set Γ_A no longer surrounds $\mathbf{0}$; it now intersects only a subset of the isochrons in $\mathcal{I}$, as can be seen for the representative case $A = 1.5$ shown in Fig. 1. Observe in panel (a) that both γ_0 and $\gamma_{0.5}$ now lie on I_0, so that now $\Delta(0) = \Delta(0.5) = 0$ in panel (b) and $\vartheta_\mathrm{n}(0) = 0$ and $\vartheta_\mathrm{n}(0.5) = 0.5$ in panel (c). Consequently, the PRC has the same (negative) sign and is of Type II, while the PTC now forms a $1:0$ torus knot, which means that it is of type

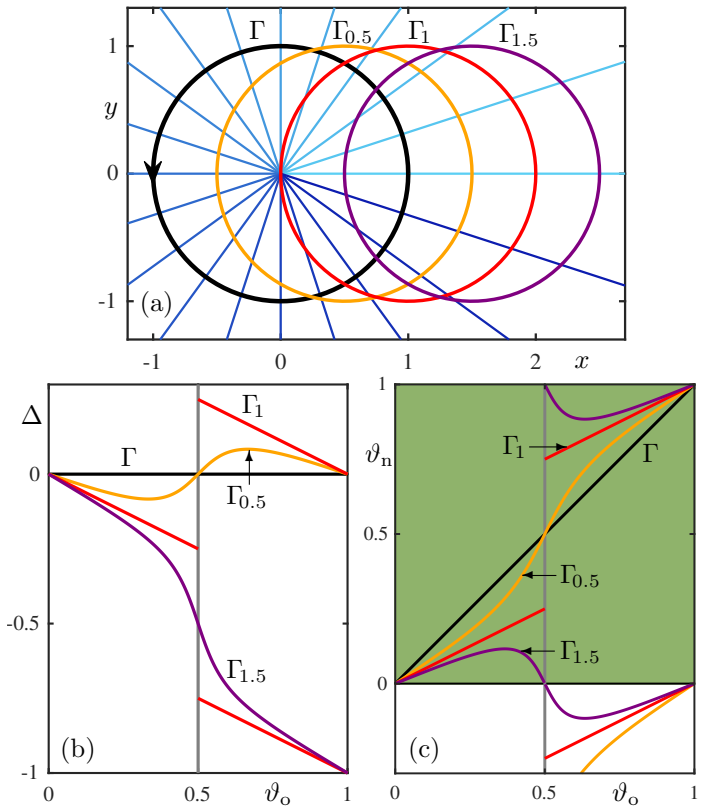

Figure 1: Phase resets with $\boldsymbol{d} = [1, 0]$ for $A = 0.5$, $A = 1$, and $A = 1.5$ in Winfree's model (7) with $\varepsilon = 0$. Panel (a) shows Γ (black) and the three perturbation sets $\Gamma_{0.5}$ (orange), Γ_1 (red), and $\Gamma_{1.5}$ (purple) together with 20 isochrons uniformly distributed in phase, which are coloured in increasingly darker shades from 0 (cyan) to 1 (dark blue). The resulting PRCs and PTCs are shown in matching colours in panels (b) and (c), respectively; the vertical line (grey) at $\vartheta_o = 0.5$ represents the discontinuity for $A = 1$, and the shaded unit square (green) in panel (c) represents $\mathbb{S}^1 \times \mathbb{S}^1$.

0 with winding number 0. This observation follows when equation (8) with $A > 1$ is written in the equivalent form

$$\sin\left(2\pi\left(\vartheta_n - \varphi_d\right)\right) = -A^{-1}\sin\left(2\pi\left(\vartheta_n - \vartheta_o\right)\right), \tag{9}$$

which shows that $\Delta = \vartheta_n - \vartheta_o$ is always positive or negative in this case, while there is a sign change of $\sin\left(2\pi\left(\vartheta_n - \varphi_d\right)\right)$.

The topological change of the PRC and PTC occurs when the perturbation amplitude is such that the perturbation set contains a point in the phaseless set. In the case of Winfree's model (as well as many other planar systems) the phaseless set is a single point, here $\mathbf{0}$, which lies on Γ_1. More specifically, $\gamma_{0.5} + [1, 0] = \mathbf{0}$, and this means that both the PRC and PTC are not defined at $\vartheta_o = 0.5$: both exhibit a discontinuity at this ϑ_o-value. In Fig. 1(b) and (c), when $A = 1$, the PRC and PTC are actually linear with slopes -0.5 and $+0.5$, respectively; as is discussed further in Sec. 2.3, this is due to the special case that the isochrons are straight rays.

Equation (8) for $0 < A < 1$ and equation (9) for $A > 1$ also explain the observed similarities between the PRCs and the PTCs in Fig. 1. Namely, they show that for $\varphi_d = 0$ the PRC for given A is exactly the 'negative' PTC for A^{-1}, defined as the graph of $-\vartheta_n(\vartheta_o)$.

Figure 2 shows a new type of reset, again for Winfree's model with $A = 0.5$, $A = 1$, and $A = 1.5$, but now for varying unit direction vector $\boldsymbol{d}$ around a given point on Γ, here, we choose $\gamma_{\vartheta_o} = \gamma_{0.125}$. We write $\boldsymbol{d} = \boldsymbol{d}(\varphi_d) := [\cos\left(2\pi\,\varphi_d\right), \sin\left(2\pi\,\varphi_d\right)]$, where $\varphi_d \in \mathbb{S}^1$, and are

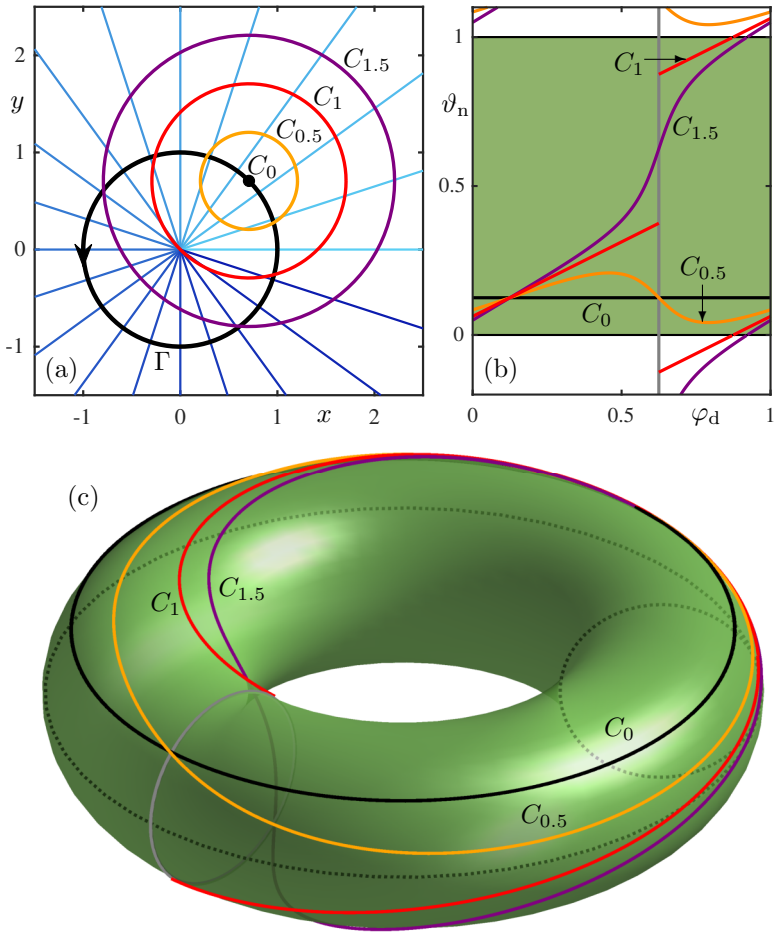

Figure 2: Directional resets of system (7) with $\varepsilon = 0$ at $\gamma_{0.125}$ for $A = 0.5$, $A = 1$, and $A = 1.5$ with $\boldsymbol{d} = [\cos(2\pi\,\varphi_\mathrm{d}), \sin(2\pi\,\varphi_\mathrm{d})]$ and $\varphi_\mathrm{d} \in \mathbb{S}^1$. Panel (a) shows Γ (black) and the three perturbation sets $C_{0.5}$ (orange), C_1 (red), and $C_{1.5}$ (purple) centred at $C_0 = \gamma_{0.125}$ (black dot) together with 20 isochrons uniformly distributed in phase, coloured from 0 (cyan) to 1 (dark blue). The resulting DTCs in matching colours are shown in the $(\varphi_\mathrm{d}, \vartheta_\mathrm{n})$-plane in panel (b) and on the torus in panel (c); the discontinuity for $A = 1$ occurs at $\varphi_\mathrm{d} = 0.625$ (grey line). Compare with Fig. 1.

interested in the new phase ϑ_n as a function of the direction angle φ_d; this is also a different circle map whose graph we refer to as the *Directional Transition Curve* (DTC). Figure 2(a) shows the periodic orbit Γ (black) and the same 20 isochrons as in Fig. 1 with the perturbation sets $C_A := \{\gamma_{0.125} + A\,\boldsymbol{d}(\varphi_\mathrm{d}) \mid \varphi_\mathrm{d} \in \mathbb{S}^1\}$ for the three values of A, which are nested circles centred at $C_0 = \gamma_{0.125}$. Panel (b) shows the three resulting DTCs, where we again show a larger range of ϑ_n with the unit square shaded. It represents the torus on which the DTCs live, which is shown in panel (c) as an embedding into $\mathbb{R}^3$.

The DTCs in Fig. 2(b) exhibits properties that are similar, yet 'dual' to those of the PTCs shown in Fig. 1(c). Namely, any perturbation set for $0 < A < 1$, such as the representative $C_{0.5}$ in panel (a), does not surround the origin $\mathbf{0}$ and the DTC is a 1:0 torus knot. The representative $C_{1.5}$ and all perturbation sets for $A > 1$, on the other hand, do surround $\mathbf{0}$, intersect all isochrons and their DTCs are 1:1 torus knots. These two different torus knots are visualised in Fig. 2(c). The topological change occurs again at $A = 1$, since $\mathbf{0} = \gamma_{0.625} + \boldsymbol{d}(0.125) \in C_1$; the DTC is then again linear with slope 0.5, but with discontinuity at $\varphi_\mathrm{d} = 0.625$. Note that, for any other value of $\vartheta_\mathrm{o} \in \mathbb{S}^1$ one finds the same DTCs modulo a corresponding translation in φ_d; this is due to

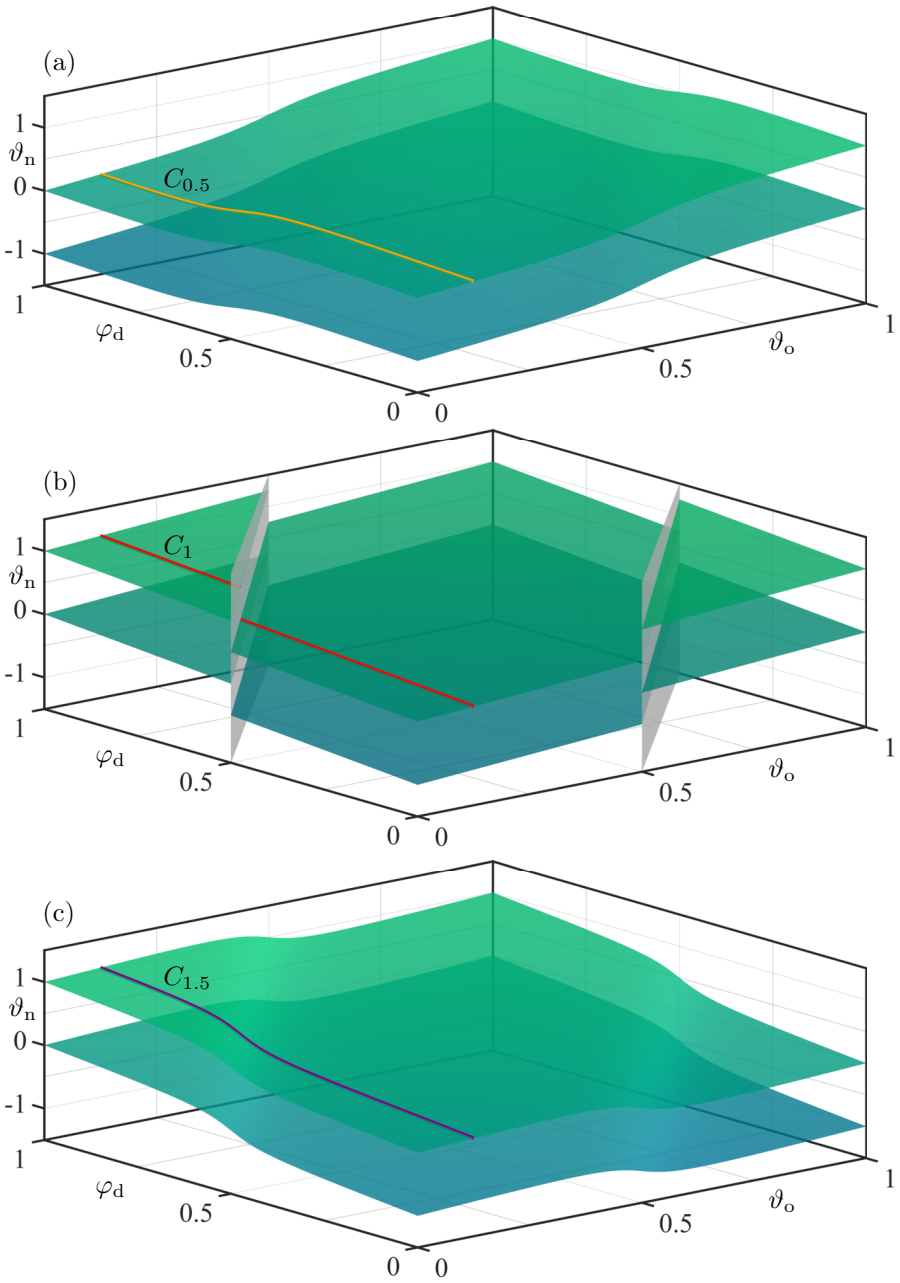

Figure 3: Resetting surface graph($\mathcal{P}_A$) of system (7) with $\varepsilon = 0$ for $A = 0.5$ in panel (a), $A = 1$ in panel (b), and $A = 1.5$ in panel (c), shown in $(\vartheta_o, \varphi_d, \vartheta_n)$-space for $\vartheta_n \in [-1.5, 1.5]$ with the corresponding DTCs for $\vartheta_o = 0.125$, labelled $C_{0.5}$ (orange), C_1 (red), and $C_{1.5}$ (purple), respectively.

the rotational invariance of this simple model. The observed duality between DTCs and PTCs for fixed $\vartheta_o = 0$ follows again from equations (8) and (9) when one considers them for fixed ϑ_o and variable φ_d: the DTC for given A is exactly the PRC for A^{-1}, subject to a translation by ϑ_o.

2.2 Resetting surfaces for straight-line isochrons

The PTC and DTC for a given amplitide A are closely related, and they correspond to different slices of the corresponding resetting surface $\text{graph}(\mathcal{P}_A) \subset \mathbb{S}^1 \times \mathbb{S}^1 \times \mathbb{S}^1$ of ϑ_n as a function of both ϑ_o and φ_d. Figure 3 shows this surface for system (7) with $\varepsilon = 0$ and the same three choices $A = 0.5$, $A = 1$, and $A = 1.5$ as in Figs. 1 and 2. In each panel of Fig. 3 we extend the range of ϑ_n to $[-1.5, 1.5]$ and show two copies of $\text{graph}(\mathcal{P}_A)$. Also shown in panels (a), (b) and (c) are the corresponding DTCs at $\vartheta_\text{o} = 0.125$ from Fig. 2(b), which are labelled $C_{0.5}$, C_1 and $C_{1.5}$, respectively.

Observe that $\text{graph}(\mathcal{P}_A)$ is a smooth surface in panels (a) and (c) of Fig. 3. The difference is that there is a phase shift by 1 in ϑ_o and none in φ_d when $0 < A < 1$, as in panel (a), while there is a phase shift by 1 in φ_d and none in ϑ_o when $A > 1$, as in panel (c). In particular, this encodes the fact that the properties of the DTCs for $\vartheta_\text{o} = 0.125$ as discussed in Sec. 2.1 also hold for DTCs for any other value of ϑ_o. The equivalent statement is true for the PTCs with φ_d fixed. In fact, it follows from equations (8) and (9) that these two surfaces are related by the duality transformation

$$(\vartheta_\text{o}, \varphi_\text{d}, A) \mapsto (\varphi_\text{d}, \vartheta_\text{o}, A^{-1}), \tag{10}$$

which is the global manifestation on the level of $\text{graph}(\mathcal{P}_A)$ of the duality between the PTCs and the DTCs. In particular, this implies the symmetry of exchanging ϑ_o and φ_d of the surface for $A = 1$ in Fig. 3(b). It features singularities at $\varphi_\text{d} - \vartheta_\text{o} = 0.5$, represented here as vertical planes in $(\vartheta_\text{o}, \varphi_\text{d}, \vartheta_\text{n})$-space, where the surface ends and has a discontinuity. Again, this encodes that any DTC for $A = 1$, such as the shown curve C_1 for $\vartheta_\text{o} = 0.125$, as well as any PTC for $A = 1$, has a discontinuity.

Since the DTC with $\vartheta_\text{o} = 0.125$ is representative for all DTCs, and due to duality also for all PTCs, we can illustrate a key property of the overall $\text{graph}(\mathcal{P})$ by showing its intersection with the different three-dimensional subspace with $\vartheta_\text{o} = 0.125$ fixed. Figure 4(a) shows this surface in $(\varphi_\text{d}, A, \vartheta_\text{n})$-space, again over the extended range $\vartheta_\text{n} \in [-0.5, 1.5]$, together with the three DTCs for $A = 0.5$, $A = 1$, and $A = 1.5$. The surface is smooth, except at the singular point $A = 1$ and $\varphi_\text{d} = \vartheta_\text{o} + 0.5 = 0.625$, where ϑ_n is undefined. This is represented in $(\varphi_\text{d}, A, \vartheta_\text{n})$-space as the vertical line, on which the surface is seen to limit in a helical fashion; in other words, the surface can be completed by the vertical line.

A key observation from equation (3) is the following: the level set for any fixed ϑ_n of the surface shown in Fig. 4(a) consists of the points in the (φ_d, A)-plane that lie on the isochron I_{ϑ_n}. Moreover, as Fig. 2 illustrates with the shown perturbation sets C_A, for fixed ϑ_o, any point in the (x, y)-plane is represented uniquely by (A, φ_d) as polar coordinates around the point $C_0 = \gamma_{\vartheta_\text{o}}$, given by the map

$$\begin{array}{rcl} \Psi : \mathbb{S}^1 \times \mathbb{R}_0^+ & \to & \mathbb{R}^2 \\ (\varphi_\text{d}, A), & \mapsto & \gamma_{\vartheta_\text{o}} + A\boldsymbol{d}(\varphi_\text{d}) = \gamma_{\vartheta_\text{o}} + [A\cos(\varphi_\text{d}), A\sin(\varphi_\text{d})]. \end{array} \tag{11}$$

While Ψ depends on ϑ_o, we do not reflect this in the notation for convenience. Its inverse Ψ^{-1} is well defined, except at the point $\gamma_{\vartheta_\text{o}}$. In particular, Ψ^{-1} is a diffeomorphism with bounded distortion near the point $\mathbf{0}$ of the phaseless set. Hence, the surface in Fig. 4(a) is the diffeomorphic image of the isochron surface in (x, y, ϑ)-space near $\mathbf{0}$, which is simply the lift of the isochrons I_ϑ for $\vartheta \in \mathbb{S}^1$. The isochron surface is shown Fig. 4(b) with the 20 straight isochrons from Fig. 2(a). Since the straight isochrons are given in polar coordinates by $\Phi(R) = \phi$ for $\varepsilon = 0$, according to (5), the isochron family $\mathcal{I}$ over the (x, y)-plane is the Riemann surface given by the graph of the argument function $\arg(\log z)/(2\pi)$ of the complex logarithm $\log(z)$, where $z = x + iy$. This implies that a single loop in the (φ_d, A)-plane around the singular point $(\varphi_\text{d}, A) = (0.625, 1)$ lifts to a helix on the resetting surface in Fig. 4(a), resulting in a phase shift by 1 in ϑ_n. Note that any helix on the isochron surface in Fig. 4(b) is anticlockwise, while

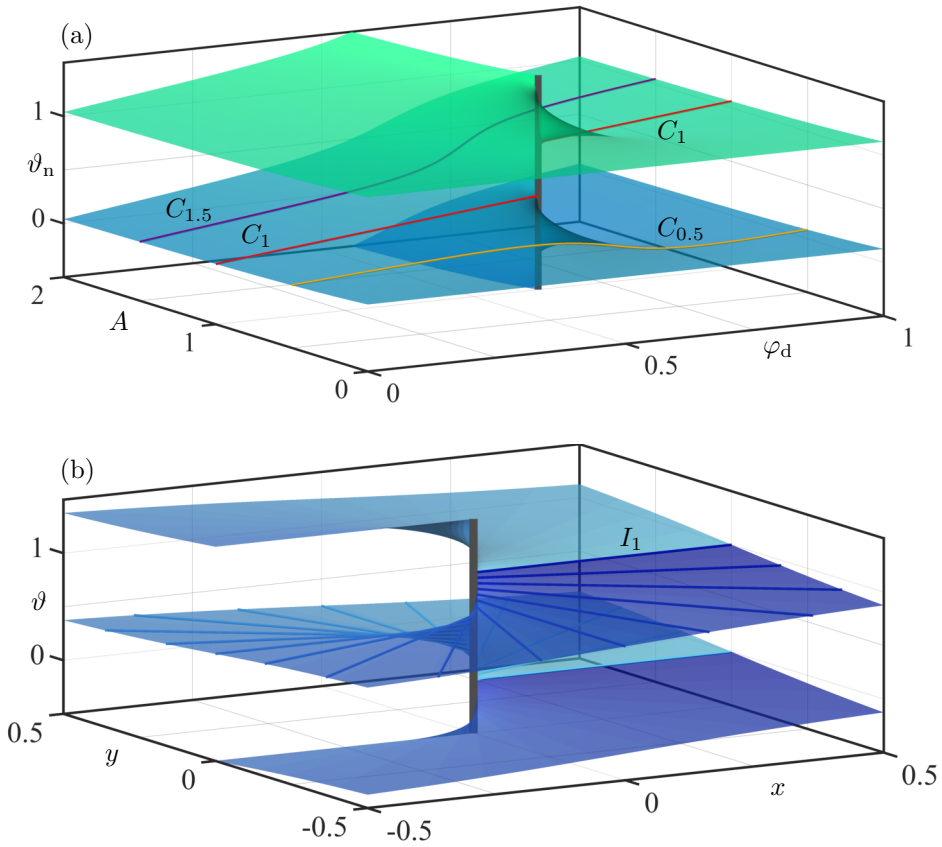

Figure 4: Resetting surface of system (7) with $\varepsilon = 0$ for fixed $\vartheta_o = 0.125$. Shown in panel (a) are two copies of the surface in $(\varphi_d, A, \vartheta_n)$-space over the range $\vartheta_n \in [-0.5, 1.5]$, as well as the corresponding three DTCs for $A = 0.5$, $A = 1$ and $A = 1.5$. The surface is discontinuous at the vertical line $\{\varphi_d = 0.625, A = 1\}$ (grey); compare with Fig. 2(b). Panel (b) shows the associated isochron surface in (x, y, ϑ)-space near $\mathbf{0}$ over the range $\vartheta \in [-0.5, 1.5]$, with the 20 straight isochrons from Fig. 2(a).

on resetting surface in Fig. 4(a) it is clockwise; this is due to the latter being the image of the former under Ψ^{-1}.

The geometry of the resetting surface encodes the qualitative change of the DTC observed in Fig. 2, namely, as the subspace for fixed A passing before, exactly through or past the singularity. In fact, the surface in Fig. 4(a) is representative for the intersection of graph($\mathcal{P}$) of system (7) with $\varepsilon = 0$ with any three-dimensional subspace of fixed φ_d or of fixed ϑ_o. Indeed, the singularity is always the implicitly defined point $\varphi_d - \vartheta_o = 0.5$ with $A = 1$, and the surfaces for fixed ϑ_o and for fixed φ_d are related by the duality transformation (10). The helical resetting surface drawn by Winfree in [47, Fig. 4] is indeed exactly the slice of graph($\mathcal{P}$) for fixed φ_d and, hence, also the diffeomorphic image of the isochron surface in Fig. 2(b).

2.3 PRC, PTC and DTC for spiralling isochrons

The case $\varepsilon = 0$ of Winfree's model (7) is helpful for illustrating the basic concepts in the simplest setting. However, it is atypical: isochrons are generally not straight lines. In particular, the period of a full rotation around the central repelling focus equilibrium is generically different from that of the surrounding periodic orbit, which means that its isochons spiral as they approach the equilibrium. This is the case for system (7) with $\varepsilon \neq 0$, and we now set $\varepsilon = -1 < 0$ as a

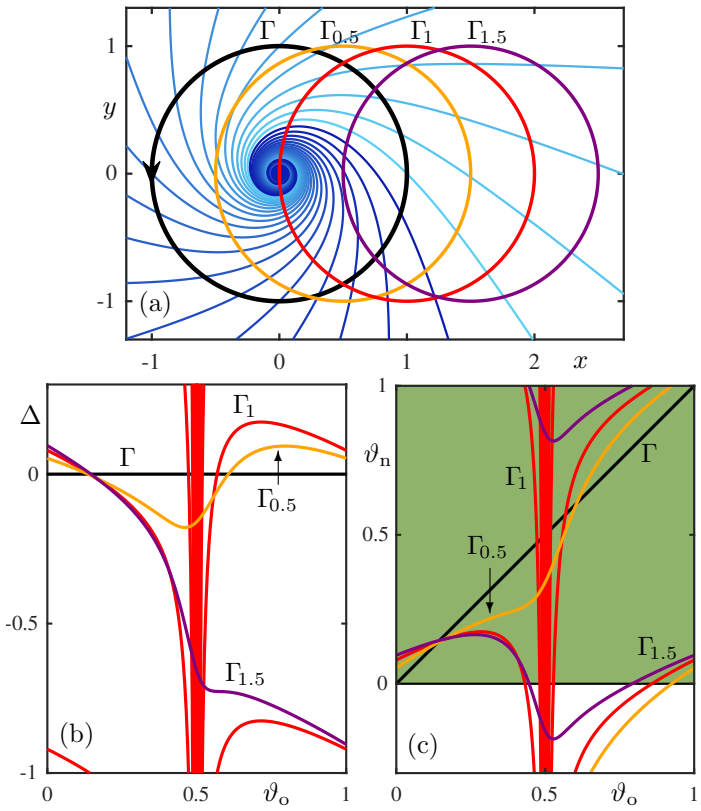

Figure 5: Phase resets with $\boldsymbol{d} = [1, 0]$ for $A = 0.5$, $A = 1$, and $A = 1.5$ in Winfree's model (7) with $\varepsilon = -1$. Panel (a) shows Γ (black), 20 isochrons uniformly distributed in phase, coloured from 0 (cyan) to 1 (dark blue), and $\Gamma_{0.5}$ (orange), Γ_1 (red), and $\Gamma_{1.5}$ (purple). The resulting PRCs and PTCs are shown in matching colours in panels (b) and (c), respectively; the discontinuity for $A = 1$ is at vertical $\vartheta_o = 0.5$, and the shaded unit square (green) in panel (c) represents $\mathbb{S}^1 \times \mathbb{S}^1$. Compare with Fig. 1.

representative example for which the isochrons spiral anticlockwise around the origin $\mathbf{0}$.

We again seek $\vartheta_n \in \mathbb{S}^1$ by finding the isochron I_{ϑ_n} that contains the perturbed point $\gamma_{\vartheta_o} + A\,\boldsymbol{d}(\varphi_d)$. As in Sec. 2.1, this leads to the expression

$$\sin\left(2\pi\left(\varphi - \vartheta_o\right)\right) = -A\,\sin\left(2\pi\left(\varphi - \varphi_d\right)\right), \tag{12}$$

but now with

$$\varphi = \vartheta_n + \frac{\varepsilon}{2\pi} - \frac{\varepsilon}{2\pi\,\|\gamma_{\vartheta_o} + A\,\boldsymbol{d}(\varphi_d)\|}, \tag{13}$$

rather than simply $\varphi = \vartheta_n$ as in (8). Again, the convention is that no solution exists if $(\vartheta_o, \varphi_d, A)$ are such that the equality holds for any $\varphi \in \mathbb{S}^1$, that is, when $\gamma_{\vartheta_o} + A\,\boldsymbol{d}(\varphi_d)$ lies at the origin.

Figures 5 and 6 illustrate that this seemingly minor variation from $\varphi = \vartheta_n$ to equation (13) has dramatic consequences. These two figures are shown in the same layout as Figs. 1 and 2; in particular, we show the respective resets for the same three values $A = 0.5$, $A = 1$, and $A = 1.5$, but now with $\varepsilon = -1$ instead of $\varepsilon = 0$.

Figure 5(a) shows Γ with 20 isochrons uniformly distributed in phase, now spiralling anticlockwise into $\mathbf{0}$, and the three perturbation sets $\Gamma_{0.5}$, Γ_1 and $\Gamma_{1.5}$. As panels (b) and (c) show, the PRCs and the PTCs for $A = 0.5$ and for $A = 1.5$ have hardly changed; compare with Fig. 1(b) and (c). However, the transition with increasing A of the PRC from Type I to Type II and the associated transition of the PTC from a 1:1 torus knot to a 1:0 torus knot, respectively, now involves an accumulation process of the DTC on the singular vertical line at $\vartheta_o = 0.5$.

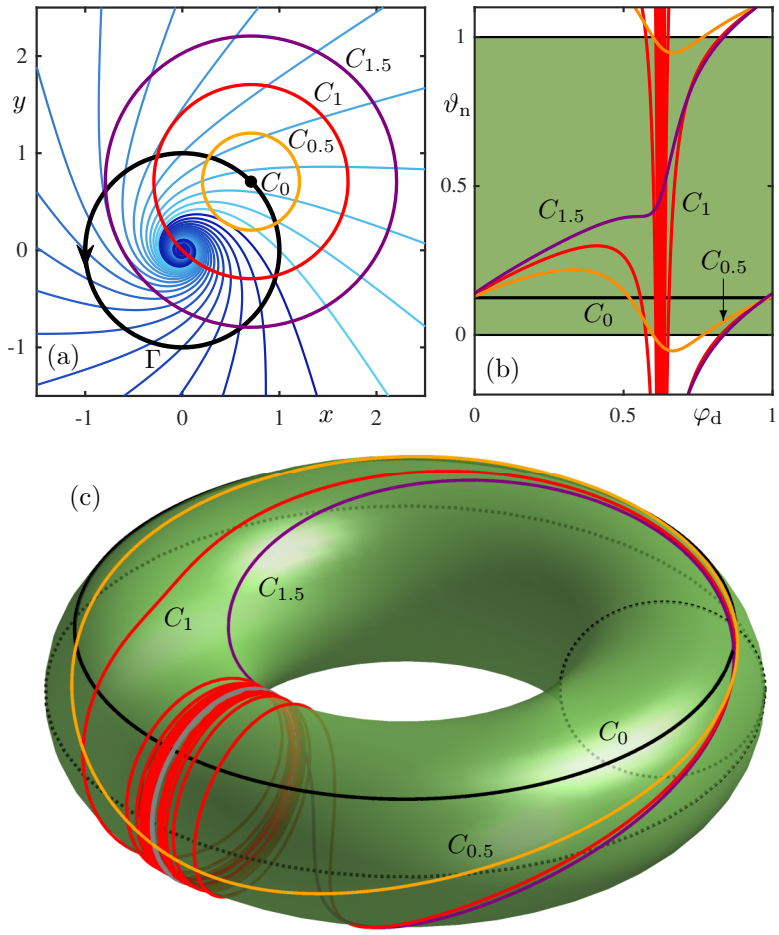

Figure 6: Directional resets of system (7) with $\varepsilon = -1$ at $\gamma_{0.125}$ for $A = 0.5$, $A = 1$, and $A = 1.5$. Panel (a) shows Γ (black) with 20 isochrons uniformly distributed in phase, coloured from 0 (cyan) to 1 (dark blue), and $C_0 = \gamma_{0.125}$ (black dot) $C_{0.5}$ (orange), C_1 (red), and $C_{1.5}$ (purple). The resulting DTCs in matching colours are shown in the (φ_d, ϑ_n)-plane in panel (b) and on the torus in panel (c); the discontinuity for $A = 1$ occurs at $\varphi_d = 0.625$. Compare with Figs. 2 and 5.

As is illustrated in Figure 6, this accumulation process is indeed also observed for the dual transition of the DTCs from a $1:0$ torus knot, as for $A = 0.5$, to a $1:1$ torus knot, as for $A = 1.5$. Panel (a) shows Γ with the 20 spiralling isochrons, together with the point $C_0 = \gamma_{0.125}$ and the three perturbation sets $C_{0.5}$, C_1 and $C_{1.5}$. The accumulation of the DTC for $A = 1$ at $\varphi_d = 0.625$ is illustrated in the (φ_d, ϑ_n)-plane in panel (b), while panel (c) illustrates it on the embedded torus; here, $\varphi_d = 0.625$ is a circle, on which the DTCs is seen to accumulate as $A \to 1$.

In both Figs. 5 and 6, the new phase ϑ_n (and, hence, also $\Delta = \vartheta_n - \vartheta_o$) grows beyond bound in the covering space $\mathbb{R}$ of $\vartheta_n \in \mathbb{S}^1$ in the limit as $A \to 1$; this is due to the fact that the respective perturbation set intersects all spiralling isochrons infinitely many times near $\mathbf{0}$. Hence, compared to the special case $\varepsilon = 0$, the PRC, PTC and DTC for $A = 1$ are markedly different for the generic case $\varepsilon \neq 0$. The consequences of the accumulation process for the geometry of graph$(\mathcal{P})$ with $\varepsilon \neq 0$ will be discussed in the next section. As we will show in Sec. 2.5, associated changes in the range of ϑ_n during the transition through $A = 1$ can be explained by what we call twin tangencies between an isochron and the perturbation set C_A.

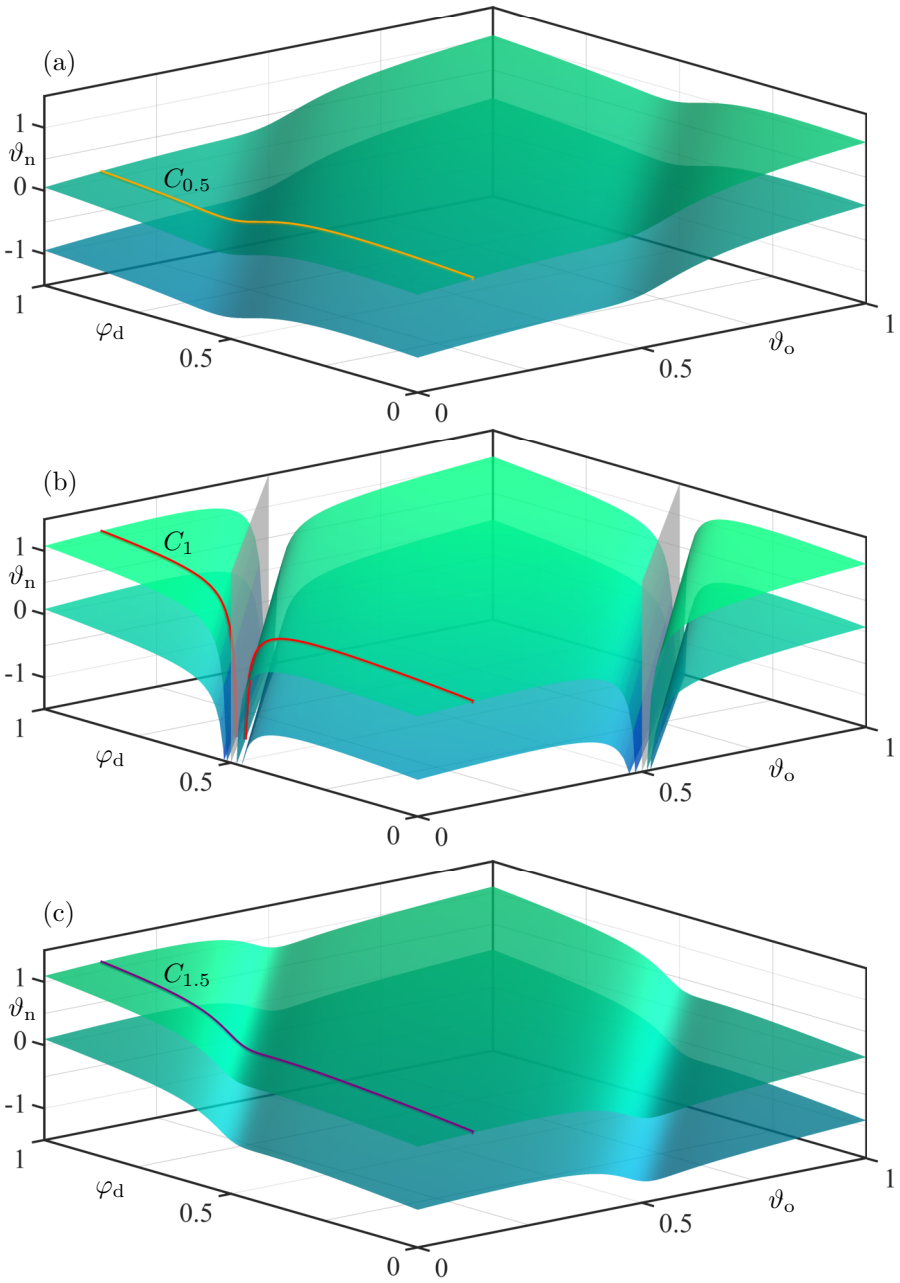

Figure 7: Resetting surface graph($\mathcal{P}_A$) of system (7) with $\varepsilon = -1$ for $A = 0.5$ in panel (a), $A = 1$ in panel (b), and $A = 1.5$ in panel (c), shown in $(\vartheta_o, \varphi_d, \vartheta_n)$-space for $\vartheta_n \in [-1.5, 1.5]$ with the corresponding DTCs for $\vartheta_o = 0.125$; compare with Fig. 3.

2.4 Resetting surfaces for spiralling isochrons

Figure 7 shows the surface graph($\mathcal{P}_A$) of system (7) with $\varepsilon = -1$ in $(\vartheta_o, \varphi_d, \vartheta_n)$-space for $\vartheta_n \in [-1.5, 1.5]$, again for $A = 0.5$, $A = 1$, and $A = 1.5$ and with the corresponding DTCs for $\vartheta_o = 0.125$. The presentation is as that in Figure 3 with $\varepsilon = 0$, so that the respective panels can be compared. Indeed, panel (a) for $A = 0.5$ and panel (a) for $A = 1.5$ look very similar. Figure 7(b), however, is significantly different and shows that graph($\mathcal{P}_A$) becomes unbounded in the direction of decreasing ϑ_n, as it approaches the singular plane $\{\varphi_d - \vartheta_o = 0.5\}$. When $\vartheta_n \in \mathbb{S}^1$ is viewed as a periodic variable, graph($\mathcal{P}_A$) makes infinitely many 'turns' around $\mathbb{S}^1$ as

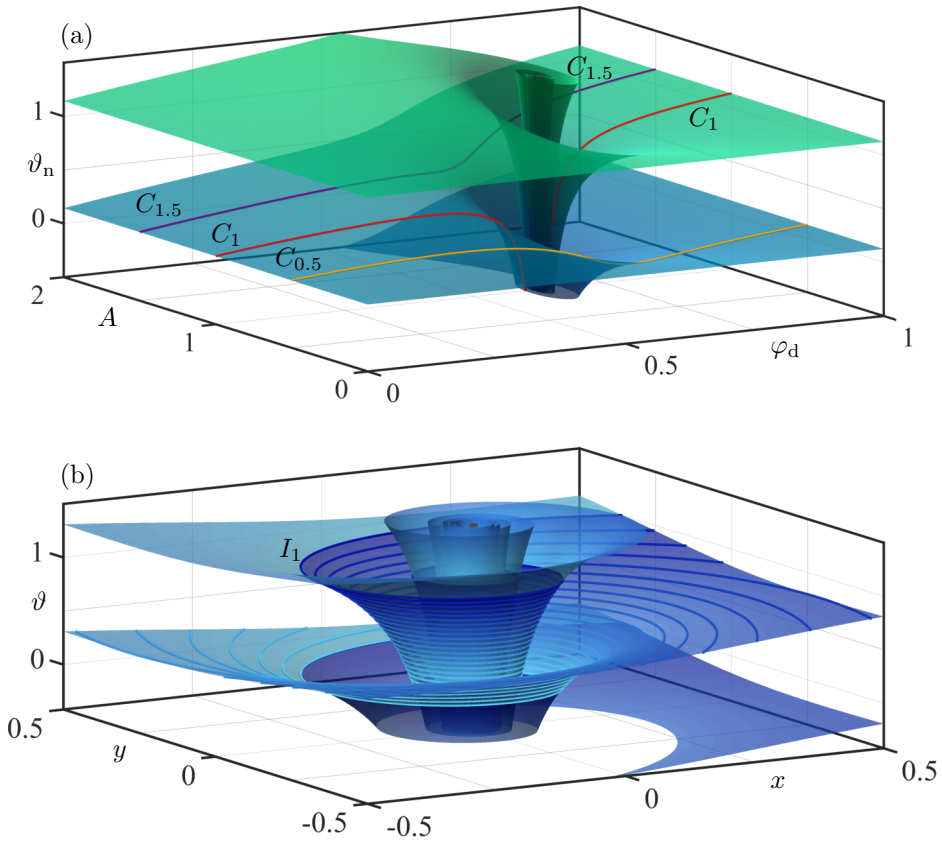

Figure 8: Resetting surface of system (7) with $\varepsilon = -1$ for fixed $\vartheta_o = 0.125$, shown in panel (a) in $(\varphi_d, A, \vartheta_n)$-space with the three DTCs for $A = 0.5$, $A = 1$ and $A = 1.5$ from Fig. 6. Panel (b) shows the associated isochron surface in (x, y, ϑ)-space near $\mathbf{0}$, with the 20 spiralling isochrons from Fig. 6(a). Compare with Fig. 4.

it approaches the singular plane from the directions of both increasing and decreasing φ_d. Note that the duality transformation (10) again applies: it relates the case for $0 < A < 1$ with that for $A > 1$, and explains the symmtry of the singular surface for $A = 1$ in Figure 7(b).

As Fig. 7 illustrates, the parameter ε has no influence on the rotational invariance of Winfree's model (7). Hence, also for $\varepsilon = -1 \neq 0$, we can again visualise the key property of graph($\mathcal{P}$) by showing its intersection with the representative three-dimensional subspace $\{\vartheta_o = 0.125\}$. Figure 8(a) shows this surface in $(\varphi_d, A, \vartheta_n)$-space over the range $\vartheta_n \in [-0.5, 1.5]$ with the three DTCs labeled $C_{0.5}$, C_1 and $C_{1.5}$ from Figs. 6 and 7. The surface is again not defined at the singularity $(A, \varphi_d) = (1, 0.625)$, which is indicated by the vertical line in Fig. 8(a). In contrast to the case with $\varepsilon = 0$ in Fig. 4, the surface does 'not end on' this vertical line, but rather 'wraps around' it.

The observation in Sec. 2.2 holds in complete generality due to the definition of the resetting map $\mathcal{P}$ by (3), and this explains the geometry of the resetting surface in Fig. 8(a): near the singularity it is the diffeomorphic image of the isochron surface, shown in panel (b), under the inverse Ψ^{-1} of the polar coordinate transformation Ψ defined in (11). Since the isochrons I_{ϑ_n} are anticlockwise spirals around $\mathbf{0}$ according to (5) with $\varepsilon = -1$, the level sets of the resetting surface are clockwise spirals. Any single closed loop in the (φ_d, A)-plane that surrounds the singularity still lifts to a curve on the surface whose end points have a phase difference of 1 in ϑ_n. However, since the phase ϑ_n is not bounded (in the covering space $\mathbb{R}$ of $\mathbb{S}^1$), this may include excursions to larger and larger negative phase and back when a curve passes closer to

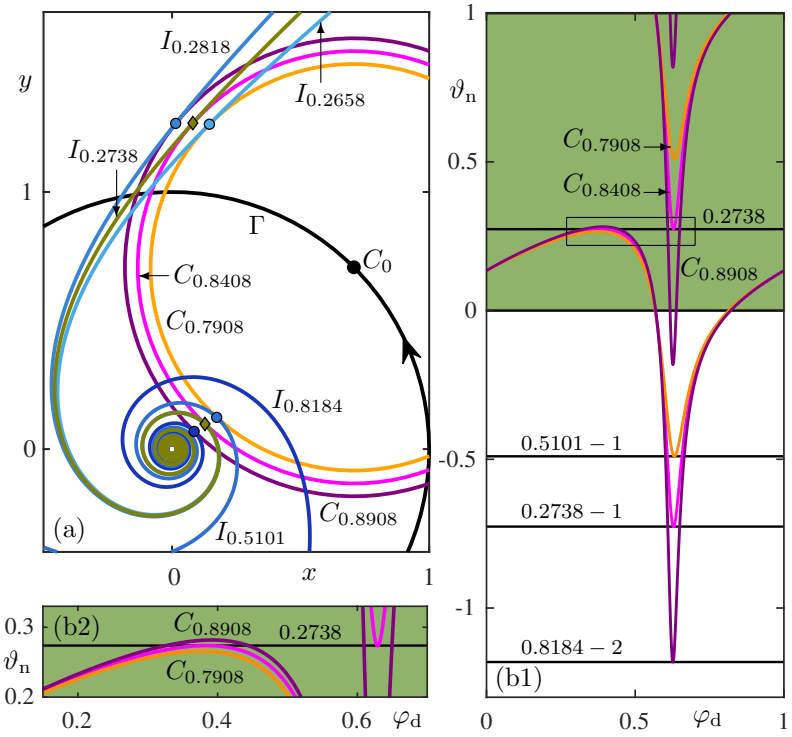

Figure 9: First twin tangency for $0 < A < 1$ of the DTC with $\vartheta_o = 0.125$ of system (7) with $\varepsilon = -1$. Panel (a) shows Γ (black) with $C_0 = \gamma_{0.125}$ (black dot) and the perturbation sets C_A for $A = 0.7908$ (orange), $A = 0.8408$ (magenta), and $A = 0.8908$ (purple), which have tangencies, respectively, with the isochrons $I_{0.2658}$ (navy) and $I_{0.5101}$ (brown), with $I_{0.2738}$ (olive) twice, and with $I_{0.2818}$ (dark green) and $I_{0.8184}$ (light green); the tangency points are marked. Panel (b1) shows the corresponding DTCs for $\vartheta_n \in \mathbb{R}$, and the highlighted rectangle is enlarged in panel (b2); here the unit square (green shading) represents $\mathbb{S}^1 \times \mathbb{S}^1$, and the ϑ_n-values of the extrema of the DTCs as indicated by horizontal lines (black).

the singular point $(\varphi_d, A) = (0.625, 1)$.

2.5 Range of the DTC and twin tangencies

The surface in Fig. 7(a) for $\varepsilon = -1$ represents the general case of a phaseless set with isochrons that spiral around an isolated point of the phaseless set. In particular, it encodes the qualitative change of the DTC: passing through the subspace for $A = 1$ leads to the transition observed in Fig. 6, from a $1:0$ torus knot, as shown with $C_{0.5}$, via the discontinuous curve C_1, to a $1:1$ torus knot, as shown with $C_{1.5}$. The reverse transition occurs for the PTC via the duality transformation (10).

Note in Figs. 6(b) and 7(a) that the DTC for $A = 0.5$ is not only a $1:0$ torus knot but, as for the limiting case for $A = 0$, it is not surjective as a circle map on $\mathbb{S}^1 \times \mathbb{S}^1$; note that this DTC is also not injective. The DTC for $A = 1.5$, on the other hand, is not only a $1:1$ torus knot but, as for limiting case $A \to \infty$ (equivalent to the PTC for $A = 0$), it is also a near-identity map; in particular, this DTC is not only surjective but also injective. For the special case $\varepsilon = 0$ of non-spiralling isochrons, these properties of the DTC hold for all $0 < A < 1$ and $A > 1$, repsectively, and the transition takes place 'suddenly' at the transition value $A = 1$. However, this is not the case when the isochrons spiral into the phaseless set $\mathbf{0}$: surjectivity is gained by the DTC with $0 < A < 1$ before $A = 1$ is reached; likewise, the DTC is injective only for sufficiently large $A > 1$. As we discuss now, these changes of the mapping properties of the DTC

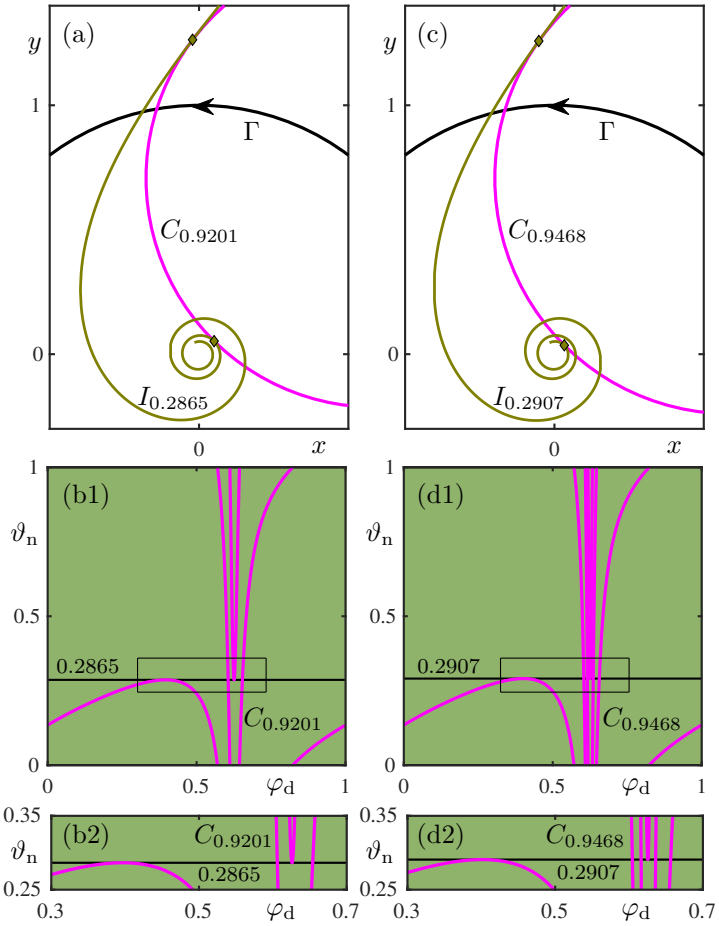

Figure 10: The second and third twin tangencies for $0 < A < 1$ of the DTC with $\vartheta_o = 0.125$ of system (7) with $\varepsilon = -1$. Panels (a) and (c) show C_A (magenta) and the twin tangency isochron (olive) with $k = 2$ at $A = 0.9201$, and with $k = 3$ at $A = 0.9468$, respectively; panels (b1) and (d1) and the enlargements in panels (b2) and (d2) show the corresponding DTCs on the unit square representing $\mathbb{S}^1 \times \mathbb{S}^1$.

are due to twin tangencies between the perturbation set C_A and the spiralling isochrons as the respective section of the resetting surface in Fig. 7(a) passes closer and closer to the singularity at $(A, \varphi_d) = (1, 0.625)$, and develops longer and longer excursions to large negative values of ϑ_n.

Figure 9 illustrates the emergence of surjectivity of the DTC of system (7) with $\varepsilon = -1$ and for fixed $\vartheta_o = 0.125$. Shown in panel (a) are Γ (black curve) together with three perturbation sets C_A for values of A just before, at, and just after this transition, together with isochrons that they are tangent to; the corresponding DTCs are shown in panel (b1) with the indicated rectangle enlarged in panel (b2). Each DTC has two extrema, a (local) maximum and a (local) minimum, which are each due to a tangency with a corresponding isochron; such a tangency is generically quadratic (see also [28]), and the respective isochrons and tangency points are shown in Fig. 9(a). The DTC becomes surjective when its minimum and maximum have the same value in $\mathbb{S}^1$ for the first time; hence, in the covering space $\mathbb{R}$ they have a phase shift by exactly 1. In terms of isochron tangencies, this means that C_A is tangent to one and the same isochron, rather than to two different isochrons; we refer to this special situation as a *twin tangency*. Figure 9 shows that it occurs for the first time (for increasing A) at $A \approx 0.8408$, where $C_{0.8408}$ is tangent to $I_{0.2738}$ at two points. For $A = 0.8408 \pm 0.05$, on the other hand, C_A is clearly tangent to two different isochrons. Note that $C_{0.8408}$ is the circle with the smallest radius that intersects

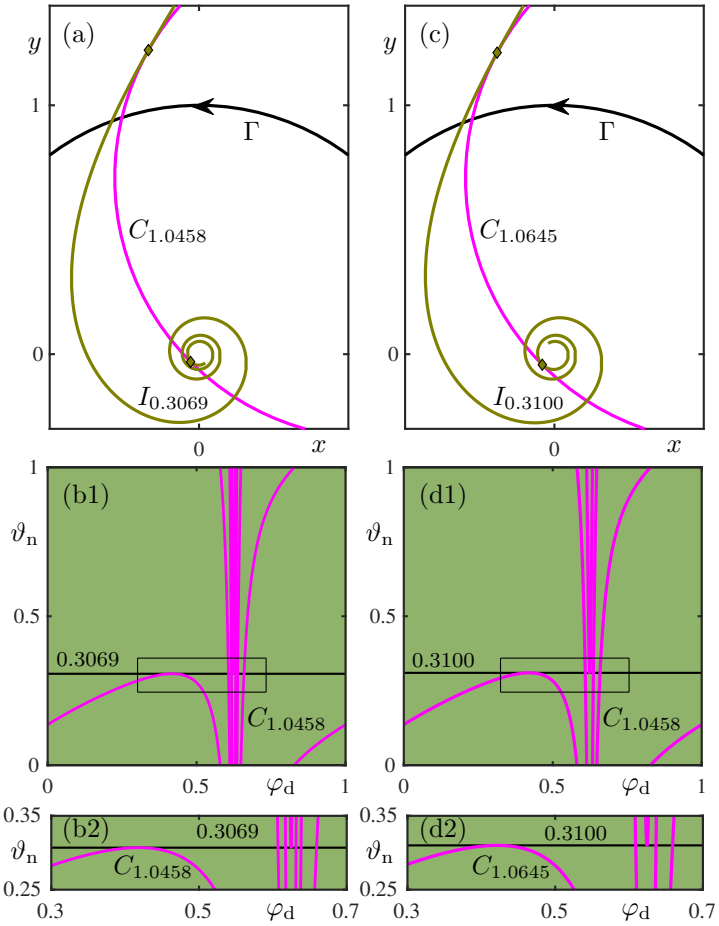

Figure 11: Twin tangencies for $A > 1$ of the DTC with $\vartheta_o = 0.125$ of system (7) with $\varepsilon = -1$, shown in the style of Fig. 10 for $\ell = 3$ at $A = 1.0458$ in panels (a) and (b), and for $\ell = 2$ at $A = 1.0645$ in panels (c) and (d).

all isochrons in $\mathcal{I}$. Hence, the DTC is surjective for $A > 0.8408$ and, since it is still a $1:0$ torus knot for $A < 1$, each value of $\vartheta_n \in \mathbb{S}^1$ is now achieved at least twice.

As A is increased, the minimum moves towards larger negative values of ϑ_n as the DTC starts to accumulate on the circle with $\varphi_d = 0.625$ in the limit of $A \to 1$, as shown in Fig. 6(c). The maximum of the DTC, however, effectively remains unchanged. Hence, there is an infinite sequence of further twin tangencies, at which the phase shift in $\vartheta_n \in \mathbb{R}$ is exactly $k \in \mathbb{N}$, so that the maximum and minimum of the DTC are again equal on $\mathbb{S}^1$. Just past the kth twin tangency the DTC covers the full range $\vartheta_n \in \mathbb{S}^1$ at least $2k$ times. Figure 10 illustrates this in panels (a) and (b) for $k = 2$ where $C_{0.9201}$ has a twin tangency with $I_{0.3100}$, and in panels (c) and (d) for $k = 3$ where $C_{0.9468}$ has a twin tangency with $I_{0.2907}$. As a result, ϑ_n covers $\mathbb{S}^1$ at least four times for $0.9201 < A < 1$, and at least six times for $0.9468 < A < 1$.

This 'increase of surjectivity' continues at infinitum since $k \to \infty$ as $A \nearrow 1$. However, the DTC remains a $1:0$ torus knot for $0 < A < 1$: it appears to increase its winding number by adding further rotations through the centre of the torus but, upon reaching its local minimum with respect to $\vartheta_n \in \mathbb{R}$, the DTC changes direction and unwinds itself before this curve closes. At $A = 1$ the DTC is singular, and this is exactly where it changes to a $1:1$ torus knot for $A > 1$. Indeed, a similar accumulation process of the DTC exists: there is now a sequence of twin tangencies for $A > 1$, where the phase shift in $\vartheta_n \in \mathbb{R}$ is exactly $\ell \in \mathbb{N}$, with $\ell \to \infty$ as $A \searrow 1$. Since it is now a $1:1$ torus knot, this means that the DTC covers the full range $\vartheta_n \in \mathbb{S}^1$

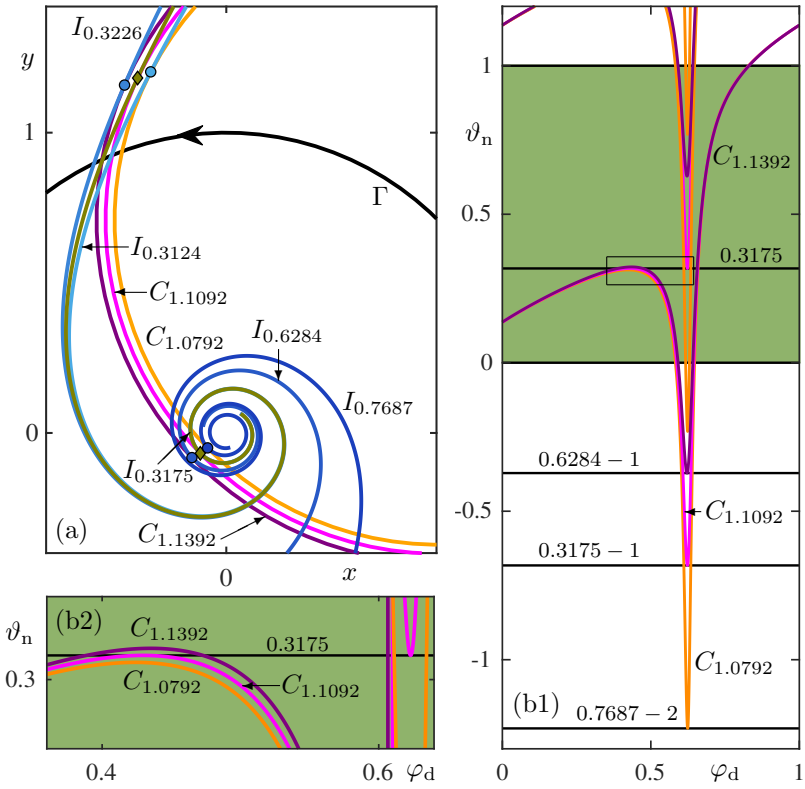

Figure 12: Last twin tangency for $A > 1$ with $\vartheta_o = 0.125$ fixed of system (7) with $\varepsilon = -1$, where $C_A = 1.1092$ is tangent twice to $I_{0.3175}$ (olive), which is shown with C_A for $A = 1.1092 \pm 0.03$ in the style of Fig. 9.

at least $2\ell + 1$ times just before the ℓth twin tangency, and only $2\ell - 1$ times just after it. In Fig. 11 we illustrate this sequence of twin tangencies with decreasing ℓ, that is, for increasing A. In panels (a) and (b) for $\ell = 3$, the perturbation set $C_{1.0458}$ has a twin tangency with $I_{0.3100}$, and in panels (c) and (d) for $\ell = 2$, $C_{1.0645}$ has a twin tangency with $I_{0.2907}$. As a result, ϑ_n covers $\mathbb{S}^1$ at least five time for $1.0458 < A < 1.0645$, while this number drops to three for $A > 1.0645$.

Figure 12 illustrates the case $\ell = 1$ of the last twin tangency for $A > 1$. Here we show the perturbations set C_A with the isochrons to which it is tangent for three values of A just before, at, and just after this twin tangency at $A \approx 1.1092$. Observe how Fig. 12 shows the reverse process of that illustrated in Fig. 9. However, the global picture is different: because the DTC is now a $1:1$ torus knot, the last twin tangency for $\ell = 1$ does not result in a loss of surjectivity. Notice that $C_{1.1092}$ in panel (a) has two tangency points with C_A and only one additional crossing; hence, the DTC in panel (b) at the nearby value of $A = 1.1392$, indeed, remains surjective.

The DTC for $A = 1.5$ in Figs. 6(b) and 7(a) is close to the identity on $\mathbb{S}^1 \times \mathbb{S}^1$, which means that it is the graph of an injective function. However, this is not the case for the DTC for $A = 1.1392$ in Fig. 12(b), because the graph still features a maximum and a minimum. The transition to injectivity occurs when the DTC has a cubic tangency (with respect to lines of constant ϑ_n), where its maximum and minimum coalesce and subsequently disappear; Fig. 13 illustrates that this happens for $A \approx 1.4931$. The perturbation set $C_{1.3}$ in panel (a), has quadratic tangencies with the isochrons $I_{0.2219}$ and $I_{0.3515}$, which correspond to the extrema of the DTC shown in panel (b). At $A \approx 1.4931$, there is a cubic tangency between $C_{1.4931}$ and $I_{0.3953}$, that is, at the value of $\vartheta_n \approx 0.3953$ of the DTC. For $A > 1.4931$, the perturbation set C_A has no tangency with any of the isochrons and, rather, intersects each isochron exactly once, as

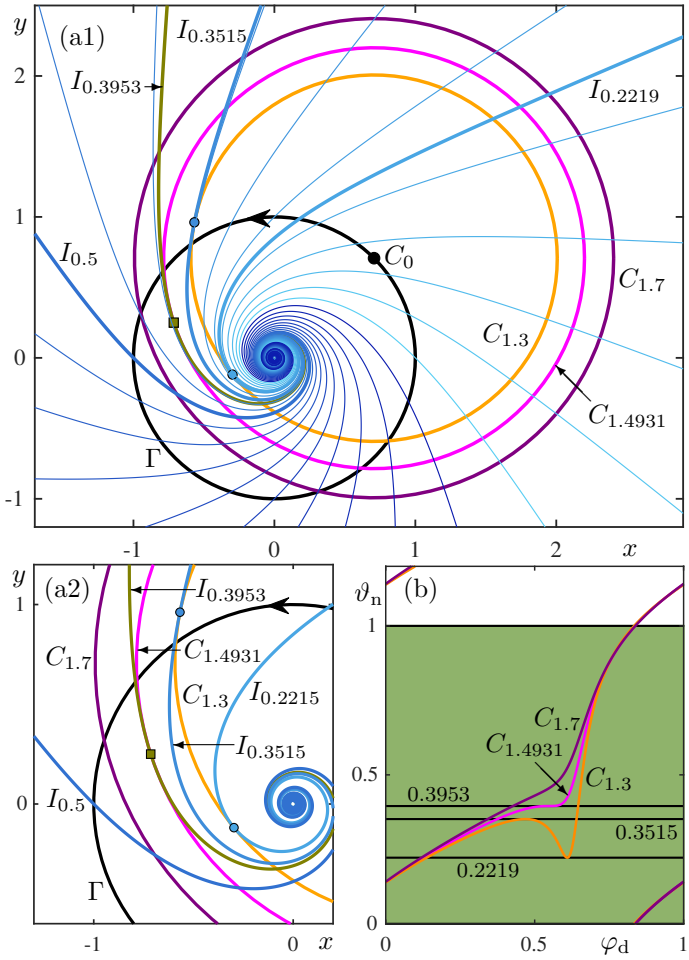

Figure 13: Transition through a cubic tangency at $A = 1.1092$ of the DTC with $\vartheta_o = 0.125$ of system (7) with $\varepsilon = -1$. Shown in panel (a1) and the enlargement panel (a2) are Γ (black), 20 isochrons uniformly distributed in phase, $C_0 = \gamma_{0.125}$, the perturbations sets C_A for $A = 1.3$ (orange), $A = 1.4931$ (magenta), and $A = 1.7$ (purple), and additional isochrons that have tangencies with them. Panel (b) shows the corresponding DTCs in matching colours for $\vartheta_n \in \mathbb{R}$, where the unit square (shaded green) represents $\mathbb{S}^1 \times \mathbb{S}^1$ and the horizontal lines (black) indcate extrema.

is the case for $C_{1.7}$ in Fig. 13. The DTC is now monotonically increasing and, indeed, the graph of an injective (and, in fact, bijective) function. We remark that successive cubic tangencies between the perturbation set and the isochron foliation have been identified in [29] as the source of additional extrema of the PTC. This is the same mechanism we found for the DTC, albeit exactly once for decreasing A.

The transition of the DTC from a 1:0 torus knot close to the constant function $\vartheta_n(\varphi_d) \equiv 0$ for small A to a 1:1 torus knot close to the identity for sufficiently large A necessarily involves the sequences of kth twin tangencies up to $A = 1$ and of ℓth twin tangencies past $A = 1$ followed by a single cubic tangency. Due to the duality transformation (10), the reverse transition through these tangencies occurs for the PTC. As we showed for the specific example of Winfree's model (7) with $\varepsilon = -1$, this scenario is entirely due to the spiralling nature of the isochrons near $\mathbf{0}$. In particular, encountering sequences of twin tangencies is a generic phenomenon when the perturbation set of a planar system transitions through an isolated point of the phaseless set around which isochrons spiral. How well this phenomenon can be observed in a given system

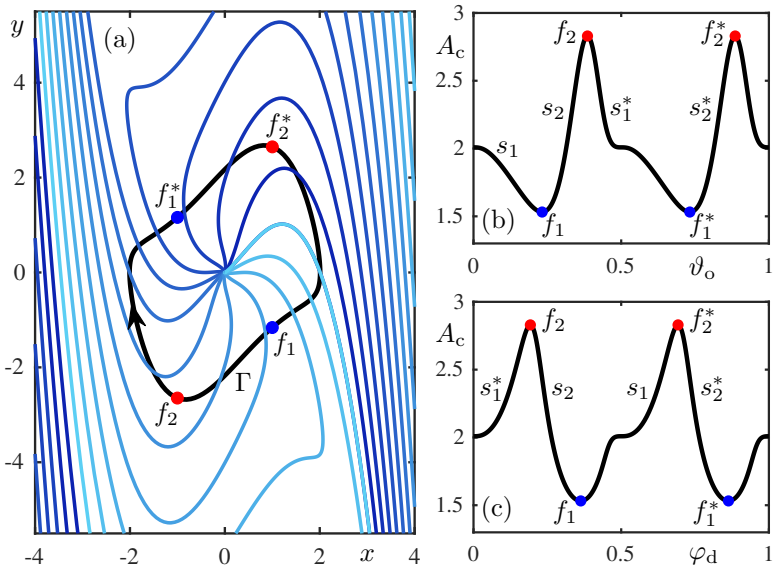

Figure 14: Periodic orbit Γ and isochron geometry of the Van der Pol system (14) with $\mu = 1$. Panel (a) shows Γ (black) with 12 isochrons evenly distributed in phase. Panel (b) shows the critical transition amplitude A_c as a function of ϑ_o, and panel (c) shows it as a function of the angle φ_d of the associated direction $\boldsymbol{d}(\varphi_d)$.

depends on how much the isochrons spiral around this point. For system (7) with $\varepsilon = -1$ the sprialling is very pronounced, and this allowed us to identify and compute twin tangencies. When ε is moved closer to 0, the spirals becomes steeper and all kth and ℓth tangencies occur increasingly closer to the singulariy $A = 1$, and they can be thought of as all 'occurring' at $A = 1$ in the exceptional case of straight-line isochrons for $\varepsilon = 0$.

3 Case study of resetting in the Van der Pol system

In this section, we consider phase resetting in the planar Van der Pol system [42, 43, 44], which we write as

$$\begin{cases} \dot{x}_1 = x_2, \\ \dot{x}_2 = \mu(1 - x_1^2)x_2 - x_1. \end{cases} \tag{14}$$

For $\mu > 0$, system (14) has a globally attracting periodic orbit Γ surrounding the origin $\mathbf{0}$, which is a repellor and the only point of the phaseless set. We fix $\mu = 1$ throughout, for which Γ has period $T_\Gamma = 6.6633$, and $\mathbf{0}$ is a focus with eigenvalues $0.5 \pm 0.8660i$ and associated period $T_{\mathbf{0}} = 2\pi/0.8660 = 7.2544$ near it. Rotation of system (14) is in the clockwise direction, and, since $T_\Gamma < T_{\mathbf{0}}$, the isochrons of Γ spiral also clockwise around $\mathbf{0}$.

The Van der Pol system is invariant under the discrete symmetry transformation

$$(x_1, x_2) \mapsto (-x_1, -x_2), \tag{15}$$

which is the rotation over π of the (x, y)-plane; hence, the periodic orbit Γ and its isochron foliation have this symmetry, but are not invariant under any other rotation. This can be seen in Fig. 14, where panel (a) shows a phase portrait with Γ and 12 isochrons that are evenly distributed in phase. The expansion near $\mathbf{0}$ in the radial direction over one period is $e^{0.5\,T_{\mathbf{0}}} \approx 37.6074$; therefore, the isochrons of Γ approach $\mathbf{0}$ so 'quickly' that it is hard to see the spiralling on the scale of Fig. 14(a). This difference notwithstanding, near $\mathbf{0}$, the isochrons of the Van der Pol system (14) are geometrically as those of Winfree's model (7) with $\varepsilon \neq 0$.

In spite of this similarity, there are a number of obvious and important differences between these two planar systems, which stem from the fact that system (14) is not invariant under any rotation about $\mathbf{0}$. In particular, the distance of a given point γ_{ϑ_o} from $\mathbf{0}$ — the phaseless set — is no longer independent of its position on Γ, as given by the phase ϑ_o. Consequently, there is a ϑ_o-dependence of the value of A required for the respective perturbation set to contain $\mathbf{0}$, when perturbed in the associated direction $\boldsymbol{d}(\varphi_d)$. More specifically, or each $\vartheta_o \in \mathbb{S}^1$ there exists a $\varphi_d \in \mathbb{S}^1$ such that this value of A is exactly the distance of γ_{ϑ_o} from $\mathbf{0}$; we refer to it as the *critical transition amplitude* $A_c = \|\gamma_{\vartheta_o}\|$ from now on. Panels (b) and (c) of Fig. 14 show A_c as a function of ϑ_o and of φ_d, respectively. Both are periodic functions that are bounded by a pair of minima, labelled f_1 and f_1^*, and a pair of maxima, labelled f_2 and f_2^*; they correspond to the points on Γ of smallest and largest distance from $\mathbf{0}$, respectively. Note that f_1 maps to f_1^*, and vice versa, under the symmetry transformation (15), and likewise for f_2 and f_2^*. Taking into account this discrete symmetry, the graphs in panels (b) and (c) are generic in the sense of Morse theory [1, 6, 35]: they have a finite number of extrema, which are locally quadratic (that is, look like parabolas). This is in marked contrast to the situation for Winfree's model, where $A_c(\vartheta_o) \equiv 1 \equiv A_c(\varphi_d)$.

The interpretation of Fig. 14(b) and (c) is the following: the point on Γ labelled f_1 ina panel (a), is given as γ_{ϑ_o} with $\vartheta_o \approx 0.2323$ lies at the minimal distance $A_c \approx 1.5317$ from $\mathbf{0}$ for a reset in the direction $\boldsymbol{d}(\varphi_d)$ with $\varphi_d \approx 0.3631$. Similarly, at the point f_2 on Γ, which is γ_{ϑ_o} with $\vartheta_o = 0.3859$, the maximal value $A_c \approx 2.8299$ is achieved for $\varphi_d \approx 0.1925$. The same is true for the points f_1^* and f_2^* subject to a shift by 0.5. For any given value A_c with $1.5317 < A_c < 2.8299$, there are four points (two symmetry-related pairs) on Γ that have distance A_c from $\mathbf{0}$; they are given by the ϑ_o-values of the points at which a horizontal line at the selected value of A_c intersects the branches s_1, s_2, s_1^* and s_2^* of the graph in panel (b). The corresponding φ_d giving the direction $\boldsymbol{d}(\varphi_d)$ of the perturbation required can be obtained from the graph in panel (c) in the same way. We conclude that singularities of graph($\mathcal{P}_A$) now occur over a range of A-values (rather than only for $A = A_c = 1$ as in Winfree's model). As we discuss next, this has consequences for the PTCs and DTCs, as well as for their associated resetting surfaces.

As Fig. 14(a) shows, the isochrons of system (14) are not simply rigid rotations of one another. Moreover, there is now no formula that parametrises them and, hence, isochrons and also PTCs and DTCs need to be computed numerically. We do so by defining suitable one-parameter families of multi-segment BVPs, which are formulated then solved within the MATLAB-based software package COCO [5]. More specifically, we compute isochrons with the COCO-implementation from [19], and PTCs and DTCs with the method from [29] (which we implemented in COCO); details can be found in Appendix A. Any resetting surfaces are rendered from the data of curves computed for a sufficient number of slices.

3.1 PTC and DTC

Figure 15 illustrates three phase resets of system (14) with $\mu = 1$ in the direction $\boldsymbol{d} = [1, 0]$, that is, with $\varphi_d = 0$, for the perturbation amplitudes $A = 1.7$, $A = A_c \approx 2.0086$ and $A = 2.3$. Panel (a) shows Γ with the 12 isochrons from Fig. 14(a) and the corresponding perturbations sets; the resulting PTCs are shown in panel (b). The perturbation set $\Gamma_{0.2}$ is close to Γ, surrounds $\mathbf{0}$ and intersect all isochrons exactly once; its PTC is not only a $1:1$ torus knot, but a near-identity transformation. At $A = A_c$ the point $\mathbf{0}$ lies on $\Gamma_{2.0086}$, and the corresponding PTC is singular at $\vartheta_o = 0.5$; as this value is approached from either side, $\vartheta_n \in \mathbb{R}$ diverges to large negative values. The computation of this singular PTC stops close to $\vartheta_o = 0.5$ on the vertical line shown in Fig. 15(b). The perturbation set $\Gamma_{3.8}$ no longer surrounds $\mathbf{0}$ and the PTC is, indeed, a $1:0$ torus knot.

Hence, these observations for the Van der Pol system agree with what we found for Winfree's

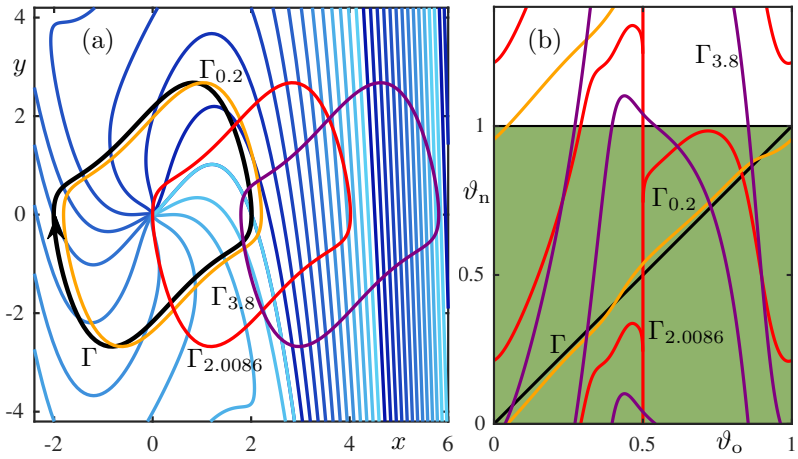

Figure 15: Phase resets with $\boldsymbol{d} = [1, 0]$ for $A = 0.2$, $A = A_c \approx 2.0086$, and $A = 3.8$ in the Van der Pol system (14) with $\mu = 1$. Panel (a) shows Γ (black), 12 isochrons uniformly distributed in phase, coloured from 0 (cyan) to 1 (dark blue), and $\Gamma_{0.2}$ (orange), $\Gamma_{2.0086}$ (red), and $\Gamma_{3.8}$ (purple). The resulting PTCs are shown in matching colours in panel (b); the discontinuity for $A = A_c$ is at $\vartheta_o = 0.5$, and the shaded unit square (green) represents $\mathbb{S}^1 \times \mathbb{S}^1$.

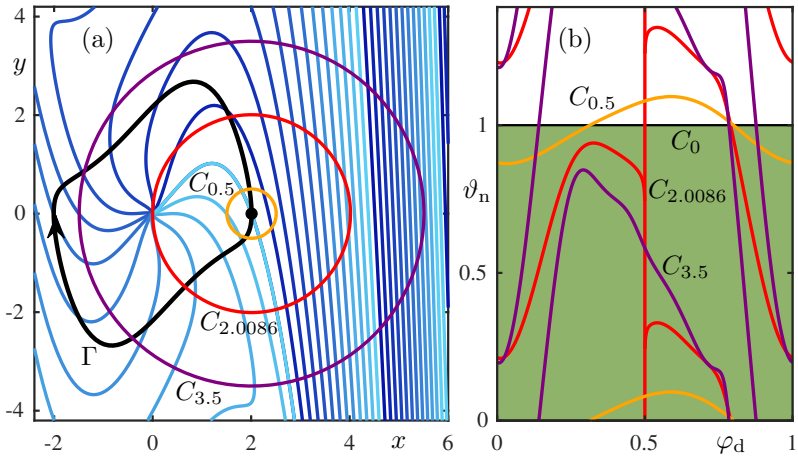

Figure 16: Directional resets of system (14) with $\mu = 1$ at γ_0 for $A = 0.5$, $A = A_c \approx 2.0086$, and $A = 3.5$. Panel (a) shows Γ (black), 12 isochrons uniformly distributed in phase, coloured from 0 (cyan) to 1 (dark blue), and $C_0 = \gamma_0$ (black dot) $C_{0.5}$ (orange), $C_{2.0086}$ (red), and $C_{3.5}$ (purple). The resulting DTCs in matching colours are shown in the (φ_d, ϑ_n)-plane in panel (b); the discontinuity for $A = A_c$ is at $\varphi_d = 0.625$. Compare with Fig. 15.

model in Sec. 2.3 with $A_c = 1$. However, there are also differences and they have to do with the structure of the isochrons outside Γ. While they spiral out evenly in Winfree's model, as shown in Fig. 5(a), they spiral out to infinity very 'unevenly' for the Van der Pol system: the isochrons make excursions to larger and larger, alternatingly positive and negative values of y. In the process they become almost vertical, and so all phases are covered in 'vertical strips' of the (x, y)-plane, as in the right-hand part of Fig. 15(a); we refer to [18] for a different but similar planar example with this geometry of the isochrons. As a result, $\Gamma_{3.8}$ intersects every isochron at least four times, which explains why the corresponding PTC is still surjective for this large value of A.

Figure 16 illustrates in the same way three directional resets centred at γ_0, that is, for $\vartheta_o = 0$. From Fig. 14(b) we know that the critical transition amplitude for the DTC is again

$A_c \approx 2.0086$, as for the PTC in Fig. 15, because this value corresponds to $\varphi_d = 0$ according to Fig. 14(c). We choose $A = 0.5$, $A = A_c \approx 2.0086$ and $A = 3.5$ in Fig. 16 for the situations before, at and after the critical transition amplitude. The perturbation set $C_{0.5}$ is close to $C_0 = \gamma_0$; it intersect only nearby isochrons. The corresponding DTC is therfore a $1:0$ torus knot, and the graph of a non-surjective function. At $A = A_c$ the DTC is singular, with ϑ_n diverging towards large negative values as $\varphi_d = 0.5$ is approached from either side. The circle $C_{3.5}$ surrounds $\mathbf{0}$ and the DTC is now indeed a $1:1$ torus knot. These observations for the DTC also agree with our findings for Winfree's model in Sec. 2.3, but there is again a difference due to the geometry of the isochrons of the Van der Pol system. As was the case for $\Gamma_{3.8}$ in Fig. 15(a), the circle $C_{3.5}$ intersects the almost vertical strips of repeating isochrons in the right-hand part of the (x, y)-plane in Fig. 16(a). Consequently, the corresponding DTC has a more complicated structure; in particular, it is not near the identity on $\mathbb{S}^1 \times \mathbb{S}^1$.

Comparison between Figs. 15(b) and 16(b) shows that the singular PTC and the singular DTC are almost identical after the transformation $\varphi_d = 1 - \vartheta_o$, that is, after reflection in the vertical line with $\vartheta_o = 0.5$ or $\varphi_d = 0.5$. Note here that the respective transition happens for the same value of $A_c \approx 2.0086$ in both cases because we consider the PTC with $\boldsymbol{d} = [1, 0]$ and the DTC around the point γ_0; see Fig. 14(b) and (c). We conclude that duality between PTC and DTC, which we found to be exact for Winfree's model as given by the transformation (10) centred at $A = 1$, still holds, to good approximation, also for the Van der Pol system centred at A_c — in spite of the fact that the perturbation set Γ_A is now no longer an actual circle (while C_A still is). We proceed by investigating what this duality means for the resetting surfaces, and the transition through sequences of twin tangencies.

3.2 Resetting surfaces

Figure 17 shows the resetting surface graph$(\mathcal{P}_A)$ for the Van der Pol system (14) with $\mu = 1$ in $(\vartheta_o, \varphi_d, \vartheta_n)$-space over the range $\vartheta_n \in [-2, 1.5]$. To illustrate its transition with A, we now show graph$(\mathcal{P}_A)$ for six values of the perturbation amplitude A. For small A, such as $A = 1.3$ in panel (a), the two sheets (ϑ_n-shifted copies) shown in this range of ϑ_n are parallel, that is, do not interact. Moreover, in any slice for fixed φ_d there is an increase of ϑ_n by 1 when ϑ_o is increased by 1, while in any slice for fixed ϑ_o there is no such increase (or decrease) when φ_d is increased by 1; this is saying that any PTC is a $1:1$ torus knot, and any DTC is a $1:0$ torus knot. For sufficiently large A, such as $A = 3$ in Fig. 17(f), the two sheets shown in this range of ϑ_n are again parallel, but there is now a decrease by 1 in ϑ_n when φ_d is increased by 1 for any slice with fixed ϑ_o, and no similar increase or decrease for slices with fixed φ_d. In other words, any PTC is now a $1:0$ torus knot, and any DTC a $1:1$ torus knot. Hence, for sufficently small and for sufficiently large A the resetting surface graph$(\mathcal{P}_A)$ shares its qualitative and structurally stable properties with the resetting surface for Winfree's model with spiralling isochrons when $0 < A < 1$ and $A > 1$, respectively; compare with Fig. 7(a) and (c).

On the other hand, the sudden transition from one case to the other in Winfree's model at $A = 1$, shown in Fig. 7(b), is due to rotational invariance and not typical for systems without this continuous symmetry. The fact that the critical transition amplitude A_c is no longer constant manifests itself by the existence of an intermediate range of A values where graph$(\mathcal{P}_A)$ is topologically different and also structurally stable. For the Van der Pol system, the dependence of A_c on ϑ_o and φ_d from Fig. 14(b) and (c) manifests itself in Fig. 17 as follows. When A has the value $A \approx 1.5317$ of the mininima f_1 and f_1^* of A_c, there are two asscociated singularities of graph$(\mathcal{P}_A)$, which are represented in Fig. 17(b) by the two vertical lines that are correspondingly labelled f_1 and f_1^* as well. Increasing A past this value, leads to the creation of two pairs of singularities of graph$(\mathcal{P}_A)$; they correspond to the four branches of A_c and are labelled s_1, s_2, s_1^*, s_2^* in Fig. 17(c) and (d). Note that, at $A \approx 1.5317$, the singularities s_1 and s_2

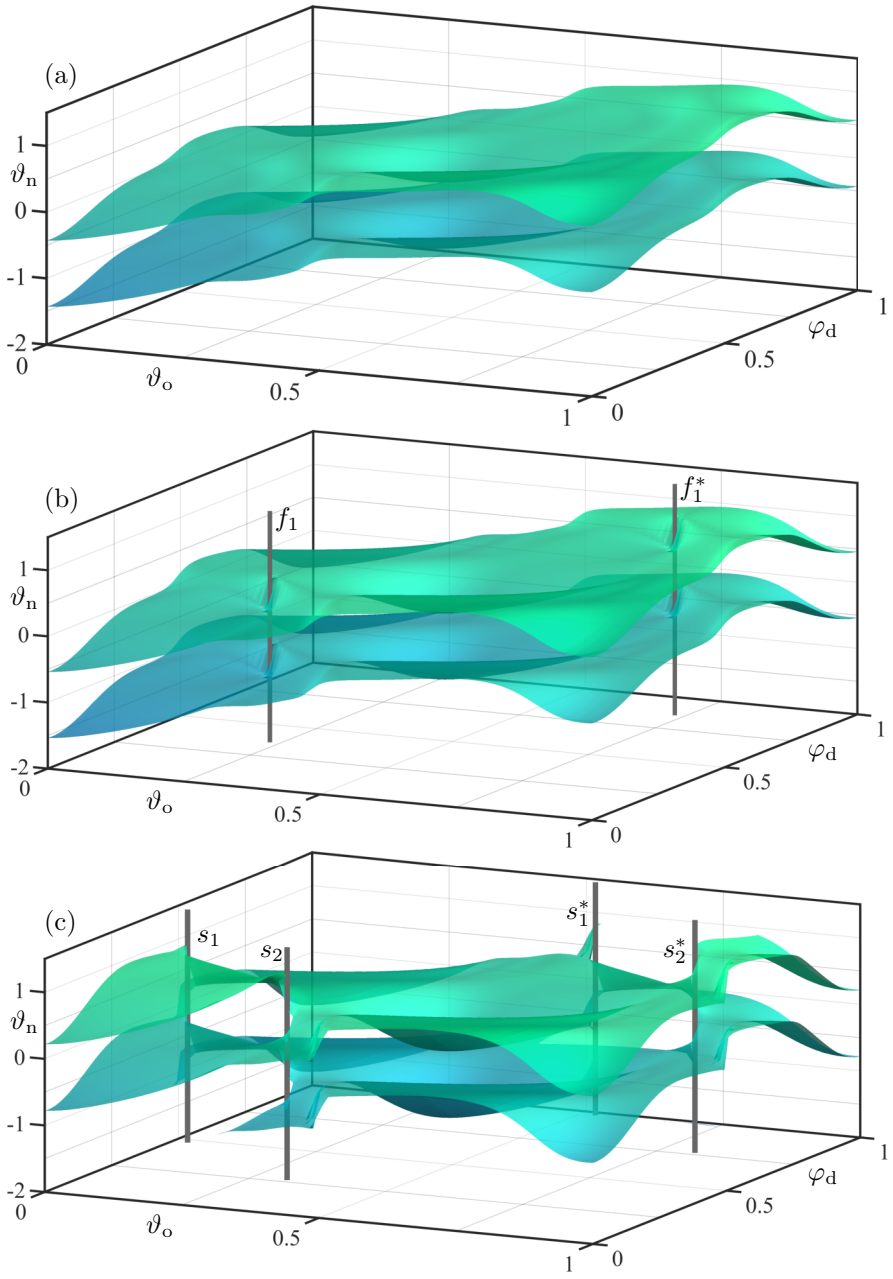

Figure 17: Resetting surface graph($\mathcal{P}_A$) of system (14) with $\mu = 1$, shown in $(\vartheta_o, \varphi_d, \vartheta_n)$-space for $\vartheta_n \in [-2, 1.5]$. Panel (a) is for $A = 1.3$, (b) for $A = 1.5317$, (c) for $A = 2$, (d) for $A = 2.3$, (e) for $A = 2.8299$, and (f) for $A = 3$. Vertical lines (grey) represent the singularities f_1 and f_1^* in (b), s_1, s_2, s_1^*, s_2^* in (c) and (d), and f_2 and f_2^* in (e); see Fig. 14(b) and (c), and compare with Fig. 7.

are created from f_1, and s_1^* and s_2^* from f_1^*; see panel (c). As A is increased further, these points drift apart and then meet again in a different constellation: s_1 moves close to s_2^*, and s_2 close to s_1^*, as is shown in panel (d). These new pairs of points meet at f_2^* and at f_2, respectively, when $A \approx 2.8299$, as shown in panel (e); indeed, this value of A is given by the corresponding maxima of A_c in Fig. 14(b) and (c). For $A > 2.8299$ there are no singularities any longer, and the transition from panel (a) to panel (f) in Fig. 17 is complete.

The intermediate case of the resetting surface graph($\mathcal{P}_A$) with singularities for $1.5317 < A <$

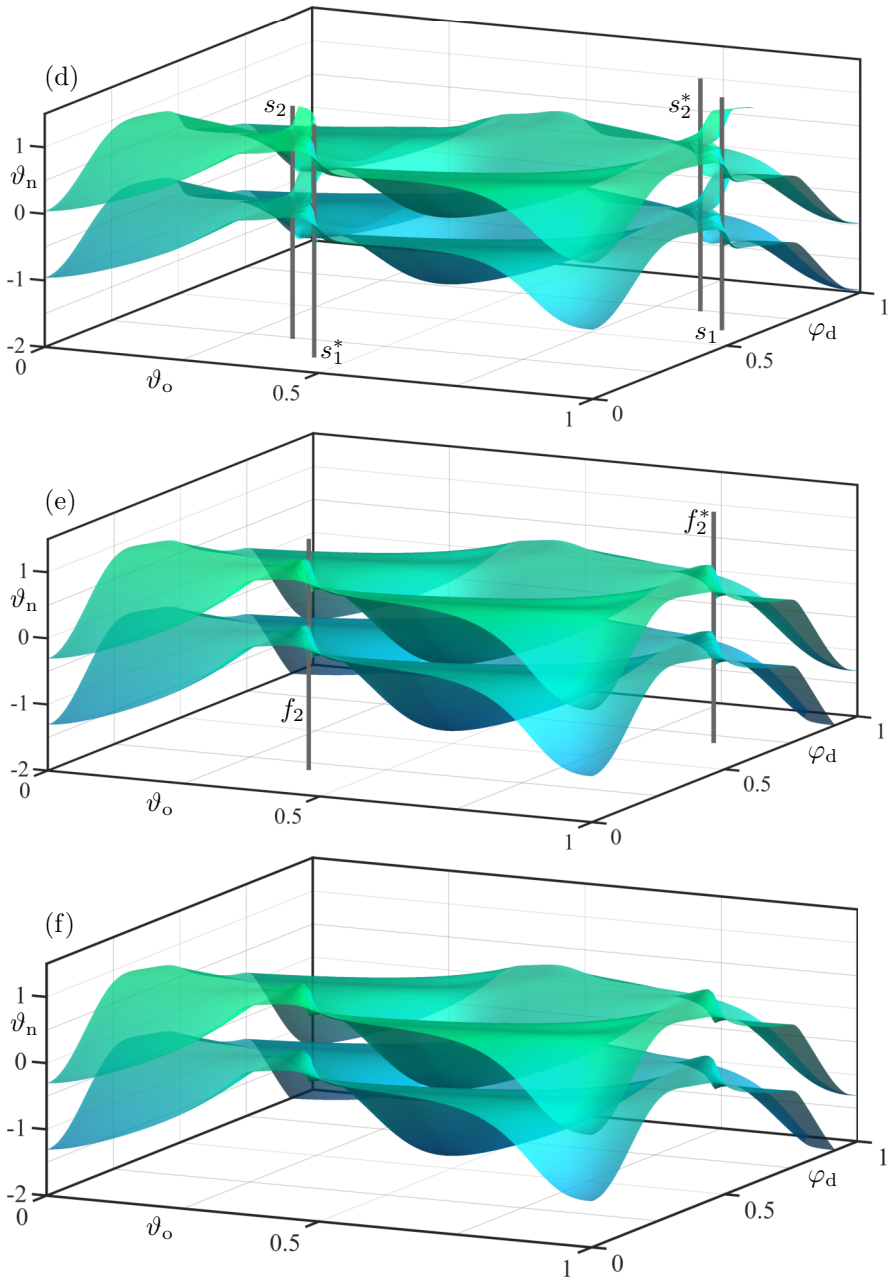

Figure 17: Continued.

2.8299 encodes the structurally stable situation when some DTCs are already 1:1 torus knots, while other DTCs are still 1 : 0 torus knots; and by duality, some PTCs are are already 1 : 0 torus knots, while others are still 1:1 torus knots. More specifically, DTCs passing between s_1^* and s_2^*, and between s_1^* and s_2^*, in Fig. 17(c) and (d) are already 1:1 torus knots; the remaining ones are still 1 : 0 torus knots, except for the four special DTCs that pass exactly through one of the singularities; the dual statement holds for the PTCs. As A is increased, there are, hence, more and more DTCs and PTCs that already changed their torus-knot type, until all of them have done so after s_1 met s_2^*, and s_2 met s_1^*, and the singularities have disappeared.

Unlike for Winfree's model, the duality between the PTC and the DTC, which we already observed in Sec. 3.1, is not exact for the Van der Pol system. Rather, it is satisfied to good

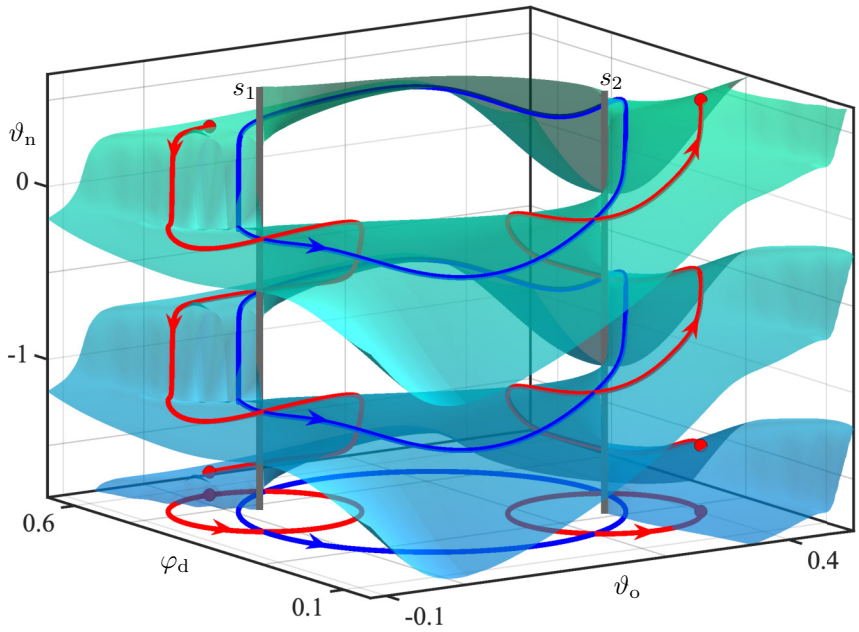

Figure 18: Enlargement of graph($\mathcal{P}_A$) for $A = 2$ from Fig. 17(c) near the singularities s_1 and s_2 (grey vertical lines), shown for $\vartheta_o \in [-0.12, 0.48]$, $\varphi_d \in [0.05, 0.65]$ and $\vartheta_n \in [-1.9, 0.7]$. Anticlockwise loops around either s_1 or s_2 in the (ϑ_o, φ_d)-plane lift, respectively, to downward and upward helices on graph($\mathcal{P}_A$) (red curves), while loops around both s_1 and s_2 lift to closed loops on graph($\mathcal{P}_A$) (blue curves).

approximation, and this can be explained by considering, for given fixed φ_d, the map

$$\begin{array}{rcl} \Theta : \mathbb{S}^1 \times \mathbb{R}_0^+ & \to & \mathbb{R}^2 \\ (\vartheta_o, A), & \mapsto & \gamma_{\vartheta_o} + A\boldsymbol{d}(\varphi_d) = \gamma_{\vartheta_o} + [A\cos(\varphi_d), A\sin(\varphi_d)]. \end{array} \tag{16}$$

The image of Θ is the 'half-strip' in the (x, y)-plane of translations of Γ in the direction $\boldsymbol{d}(\varphi_d)$; in particular, this map is neither surjective nor injective. Nevertheless, when Θ is restricted to a neighbourhood of $\mathbf{0}$, it is invertible, since the distance of Γ to the phaseless set is positive. Hence, Θ is locally a diffeomorphism and the 'dual' of the map Ψ from (11) near $\mathbf{0}$. The difference between the two maps lies in whether ϑ_o or φ_d is the input variable. Indeed, exchanging the roles of ϑ_o and φ_d means considering different and perpendicular slices through the resetting surface graph($\mathcal{P}_A$), that is, switching between considering PTCs versus DTCs.

The resetting surface graph($\mathcal{P}_A$) for $1.5317 < A < 2.8299$ crucially features the interaction near the singularities between its sheets (ϑ_n-shifted copies). The corresponding topology and geometry is illustrated in Fig. 18, which shows enlargements near s_1 and s_2 of the surfaces for $A = 2$ in Fig. 17(c). Near each singularity the surface graph($\mathcal{P}_A$) in Fig. 18 is helical, with the same local geometry as that shown in Fig. 8. However, the 'wrapping' of the surface around line of singularities in Fig. 18 is so 'sudden' (due to the fast approach of the isochrons to $\mathbf{0}$) that it cannot be seen in Fig. 18; this is why graph($\mathcal{P}_A$) near s_1 and s_2 looks rather like the case for non-spiralling isochrons shown in Fig. 4. Nevertheless, the key property is that the geometry of graph($\mathcal{P}_A$) in the covering space of ϑ_n is locally akin to a parking garage with two helical ramps of different orientation in between its parking levels. As Fig. 18 illustrates, any anticlockwise loop in the (ϑ_o, φ_d)-plane around just s_1 lifts on graph($\mathcal{P}_A$) to a downward helix, while one around just s_2 lifts to an upward helix — each connecting a 'level' of graph($\mathcal{P}_A$) with the one below or above, respectively. A closed loop in the (ϑ_o, φ_d)-plane around both s_1 and s_2, however, lifts to closed a family of loops on graph($\mathcal{P}_A$), that is, does not result in a change

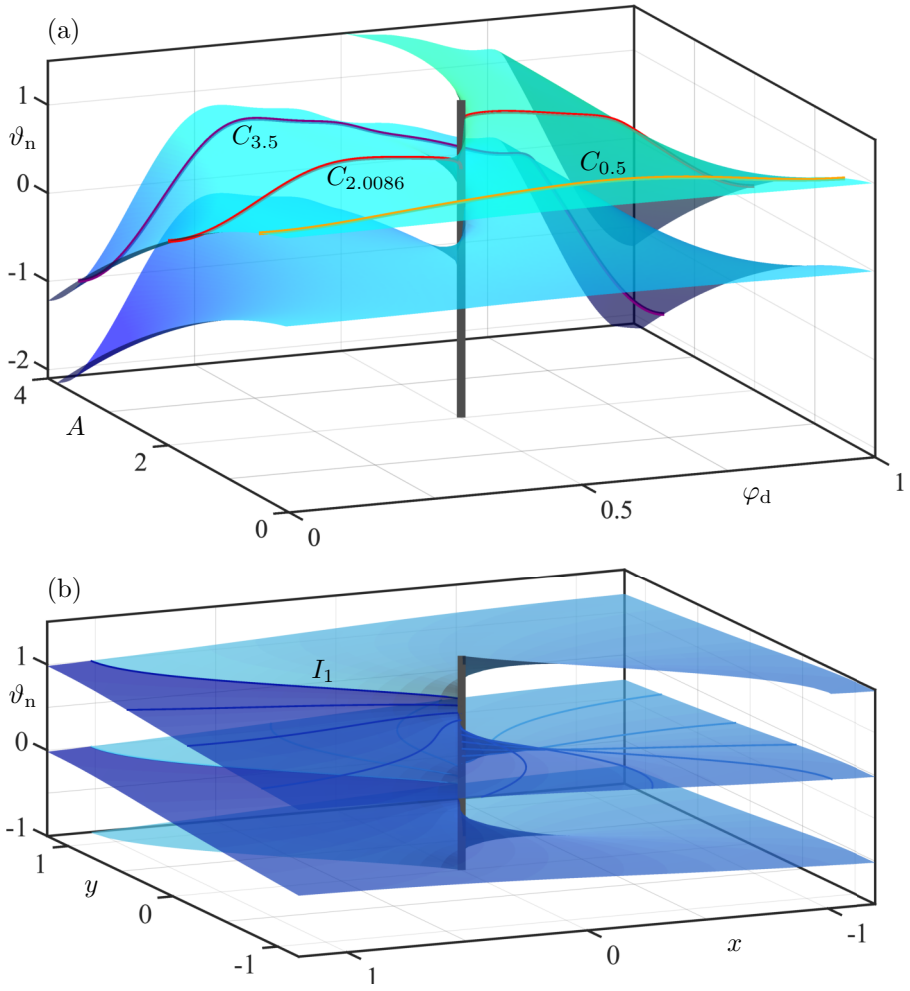

Figure 19: Resetting surface of system (14) with $\mu = 1$ for fixed $\vartheta_o = 0$, shown in panel (a) in $(\varphi_d, A, \vartheta_n)$-space with the DTCs for $A = 0.5$, $A = 2.0086$ and $A = 3.5$ from Fig. 16. Panel (b) shows the associated isochron surface in (x, y, ϑ)-space near $\mathbf{0}$, with the 12 spiralling isochrons from Fig. 14(a). Compare with Fig. 8.

of level. In particular, this means that s_1 and s_2 can indeed meet at f_1 and then disappear as A is decreased. Since, s_1^* is also a downward helix, the situation near s_2 and s_1^* is completely equivalent and, hence, this pair of singularities can also meet and disappear, namely at f_2 as A is increased. These qualitative changes are both due to the transition through a regular extremum of a Morse function and, hence, generic bifurcations of graph$(\mathcal{P}_A)$.

Figure 19 illustrates the resetting surface given by the slice of graph$(\mathcal{P})$ for fixed $\vartheta_o = 0$. Panel (a) shows it in $(\varphi_d, A, \vartheta_n)$-space with its singularity at $(\varphi_d, A) = (0.5, 2.0086)$. The DTCs from Fig. 16(b) are shown on the surface, illustrating in a different way how their transition across the singularity with A changes them from a $1:0$ to a $1:1$ torus knot. This resetting surface in Fig. 19(a) is again the image under the inverse of Ψ from (11) of the isochron surface of the Van der Pol system, which is shown in panel (b). Again, the spiralling nature of the isochrons is hardly visible at this scale, but this surface is geometrically like that in in Fig. 8(b) for Winfree's model (7) with $\varepsilon = -1$, except that the direction of spiralling is reversed. Notice, that there are some differences further away from the singularity between Fig. 19(a) and Fig. 8(a), due to the different overall isochron structure of the Van der Pol system.

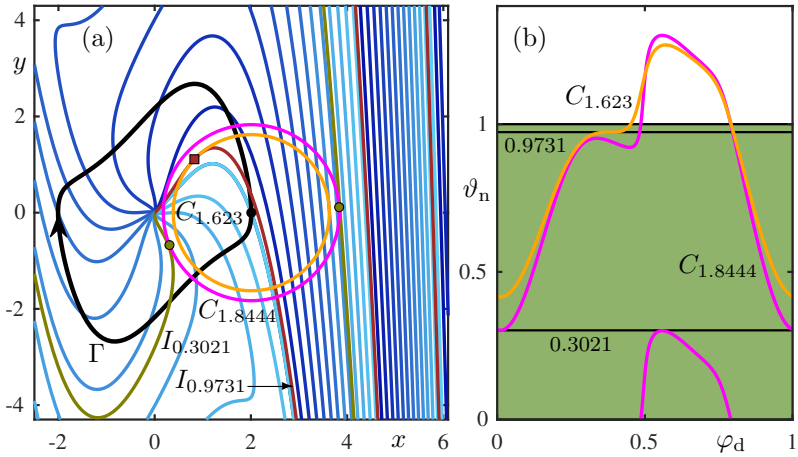

Figure 20: Twin tangency at which the DTC for $\vartheta_o = 0$ of system (14) with $\mu = 1$ becomes surjective, and nearby cubic tangency. Panel (a) shows in the (x, y)-plane that $C_{1.8444}$ (magenta) has two tangencies with $I_{0.3021}$ (olive), and $C_{1.623}$ (orange) has a cubic tangency with $I_{0.9731}$ (brown). The corresponding DTCs are shown in the (φ_d, ϑ_n)-plane in panel (b).

3.3 Twin tangencies

The Van der Pol system (14) with $\mu = 1$ becomes surjective at the twin tangency shown in Fig. 20, which occurs at $A \approx 1.8444$. Panel (a) shows that the perturbation set $C_{1.8444}$ has two tangencies with $I_{0.3021}$, and the DTC in panel (b) has a maximum and a minimum that coincide at $\vartheta_n \approx 0.3021 \in \mathbb{S}^1$. Notice that $A = 1.8444$ is quite far from the critical transition value $A_c \approx 2.0086$ and that both extrema look locally like parabolas that are not very steep. Moreover, the minimum is not near $\varphi_d = 0.5$ but near $\varphi_d = 0$, that is, the corresponding tangency with $I_{0.3021}$ in Fig. 20(a) occurs near the rightmost point of $C_{1.8444}$, where the isochrons form parallel, almost straight curves.

While the twin tangency at $A \approx 1.8444$ is responsible for the loss of surjectivity of the DTC, it is not actually part of the sequence of twin tangencies near $\mathbf{0}$ that we discussed for Winfree's model in Sec. 2.5. Rather, this sequence involves a second pair of a maximum and minumum of the DTC for $A = 1.8444$ near $\vartheta_n = 0.9$. This pair is created at the cubic tangency between $C_{1.623}$ and $I_{0.9731}$ that is also shown in Fig. 20. We remark that these additional extrema of the DTC for $A > 1.623$ arise because of a property that is not shared by the spiralling isochrons of Winfree's model: the isochrons of the Van der Pol system spiral near Γ in an anticlockwise direction before they reach a small neighbourhood of $\mathbf{0}$, around which they spiral in a clockwise direction.

While the resetting surface in Fig. 19(a) is geometrically as that of Winfree's model in Fig. 4(a), the isochrons of the Van der Pol system (14) for $\mu = 1$ form spirals near $\mathbf{0}$ that are much steeper. As a result, the corresponding sequence of twin tangencies for increasing k as $A \nearrow A_c$, and that for increasing ℓ as $A \searrow A_c$, occur in the Van der Pol system extremely close to the critical transition value A_c. Nevertheless, they do exist, as Fig. 21 illustrates.

More specifically, Fig. 21(a) shows the DTC for $A = 2.00861986$; it has still two (local) minuma and two (local) maxima as in Fig. 20(a), but the minimum near $\varphi_d = 0.5$ has moved to lower values of $\vartheta_n \in \mathbb{R}$. Both maxima in Fig. 21(a) remain clearly parabola-like, but the 'excursion' of the DTC near $\varphi_d = 0.5$ occurs over a tiny φ_d-interval and this minimum is very 'sharp'. Note that it is at $\vartheta_n \approx 0.4272$, while the corresponding maximum near $\varphi_d = 0.4$ is at $\vartheta_n \approx 0.9396$; hence, the first twin tangency with $k = 1$ has not yet occured, and the DTC is geometrically as the DTC for $A = 0.7908$ of Winfree's model that is shown in Fig. 9(b1).

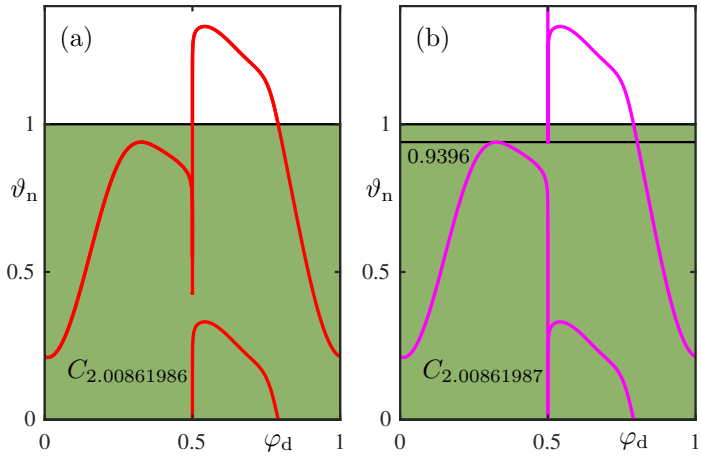

Figure 21: DTCs for $\vartheta_o = 0$ of system (14) with $\mu = 1$ extremely close to and on either side of the critical transition value A_c. Panel (a) show sthe DTC in the (φ_d, ϑ_n)-plane for $A = 2.00861986$ just before the first twin tangency with $k = 1$, and panel (b) shows it for $A = 2.00861987$ at the last twin tangency with $\ell = 1$. Compare with Fig. 9(b1) and Fig. 12(b1), respectively.

However, the DTC in Fig. 21(a) is the last (for increasing A) that we can compute and that is still a $1:0$ torus knot. Figure 21(b) shows the DTC at $A = 2.00861987$, which is now a $1:1$ torus knot with an equally sharp minimum. Note that this DTC is actually at the last twin tangency with $\ell = 1$, since its sharp minumum and the maximum near $\varphi_d = 0.4$ have the same value of $\vartheta_n = 0.9396 \in \mathbb{S}^1$; this situation is geometrically as that for $A = 1.1092$ in Fig. 12(b1). Therefore, we can state that $A_c \approx 2.00861986$ is our best estimate for the critical transition value.

It is clear from these subtle computational results that the ϑ_n-value of the minimum near $\varphi_d = 0.5$ depends extremely sensitively on A near A_c; indeed, the DTCs shown in Fig. 21 are right at the limit of what can be achieved numerically.

4 Discussion and outlook

We considered a stable periodic oscillation, represented by an attracting periodic orbit Γ of a vector field, subject to a perturbations at phase ϑ_o of the oscillation with *any* amplitude A and in *any* direction $\boldsymbol{d}$. The resulting phase ϑ_n, after transients have died down, is encoded by the phase resetting hypersurface graph$(\mathcal{P})$ of the resetting function $\vartheta_n = \mathcal{P}(\vartheta_o, \boldsymbol{d}, A)$. This generalises the notions of phase response and phase transition curves, which are obtained by fixing $\boldsymbol{d}$ and A.

We demonstrated the benefits of this extended and geometric approach to phase resetting with two planar examples: a constructed, rotationally invariant model due to Winfree, where the isochrons are known analytically, and the Van der Pol system, which needs to be investigated numerically. For the planar case, slices of graph$(\mathcal{P})$ for fixed A or for fixed ϑ_o are two-dimensional surfaces in this case, and we showed how they provide overall geometric insight into the phase resetting properties of the given oscillating system. Singularities of these surfaces arise when the perturbation lies on the boundary of the basin of attraction of the periodic orbit, which is the single repelling focus $\mathbf{0}$ for our examples. As we showed, the respective resetting surface near any such singularity is the diffeomorphic image of the isochron surface near the phaseless set $\mathbf{0}$. This general statement explains, in particular, the duality between the PTCs and the DTCs locally near their change of type, that is, from $1:1$ to $1:0$ torus knot, and vice versa. We remark that Winfree's helical surface in [47, Fig. 4] is mathematically the case of straight-line isochrons

— or, in practice, hardly spiralling isochrons. Generically, isochrons do spiral into a repelling focus, and we showed that this implies the existence of associated sequences of twin tangencies on either side of the critical transition value.

Winfree's model is representative near $\mathbf{0}$ for the case that the period of the periodic orbit is different from that of the repelling focus and the isochrons are actual spirals around it. This statement follows from the fact that (according to the Hartman-Grobmann theorem) the dynamics is practically linear sufficiently close to the focus: in this limit, the isochrons are indeed logarithmic spirals that map to each other under rigid rotations, as in Winfree's model. This configuration of isochrons can be found, in particular, past a Hopf bifurcation of the focus that generates the attracting periodic orbit; see also [28].

On the other hand, Winfree's model is very special because its rotational invariance holds globally, and not just locally near $\mathbf{0}$. In particular, its periodic orbit Γ is an exact circle around $\mathbf{0}$, and this is not representative of general planar systems. Generically one expects the distance of points on Γ to the repelling focus to be a smooth periodic function with isolated maxima and minima. This is indeed the case for the Van der Pol system, and we explained the consequences of this loss of symmetry: the resetting surface now has singularities for a range of perturbation amplitudes, between well-defined minimal and maximal values, where they (dis)appear in pairs at regular folds. The Van der Pol system is also typical in that its isochrons do not have analytic expressions and, hence, need to be computed numerically. The same is indeed also true for the PTCs, DTC and associated resetting surfaces. This is not an impediment to the approach taken here: as we demonstrated, these objects, including surfaces with several singularities, can be computed efficiently and accurately with a BVP setup. Finding the associated twin tangencies, however, is a real challenge in this case, because the spiralling nature of the isochrons of the Van der Pol system is hardly discernible near $\mathbf{0}$.

We believe that it will be interesting to study and represent resetting behaviour via resetting surfaces also in other oscillatory systems. Even for the planar case, the isochron structure near the basin boundary may be much more complicated. Already when the boundary is still a single repelling equilibrium, the isochrons near it need not be simple spirals. Rather, they can feature sudden turns, also referred to as boomerang turns [27, 33]. This phenomenon typically arises in the presence of slow-fast dynamics, and it has been explained by the existence of quadratic tangencies between the simultaneously existing foliations by the (forward-time) isochrons of the attracting periodic orbit and by the (backward-time) isochrons of the repelling focus; see [28] for details. The geometry of isochrons when the basin boundary consists of more than a single point is discussed in [18] by means of a case study of a family of planar vector fields that is also invariant under rotation by π, just as the Van der Pol system. The resetting surfaces in this setting will be interesting objects of study, since their local geometry encodes and reflects how the isochrons accumulate on such a more complicated phaseless set.

Understanding phase resetting geometrically in systems of dimension at least three is a challenge that may also be addressed in the general spirit of the approach taken here; see also [29]. Parametrising the vector $\boldsymbol{d}$ now requires at least two angles and, hence, graph($\mathcal{P}$) is higher-dimensional. Nevertheless, and possibly guided by what is perturbation can be generated in a particular application context, one may restrict $\boldsymbol{d}$ to lower-dimensional subsets, so that corresponding slices of graph($\mathcal{P}$) are still actual two-dimensional resetting surfaces consisting of PTCs and DTCs. Their geometric properties will reflect certain aspects of the phase response. In particular, singularities on resetting surfaces encode how (intersection sets of) higher-dimensional isochrons accumulate on (intersection sets of) parts of the basin boundary. Our numerical tools can be employed in this higher-dimensional setting, and our ongoing work concerns phase resetting in the three-dimensional Yamada model of a self-pulsing laser [10, 50] and in a four-dimensional example of two coupled Van der Pol oscillators.

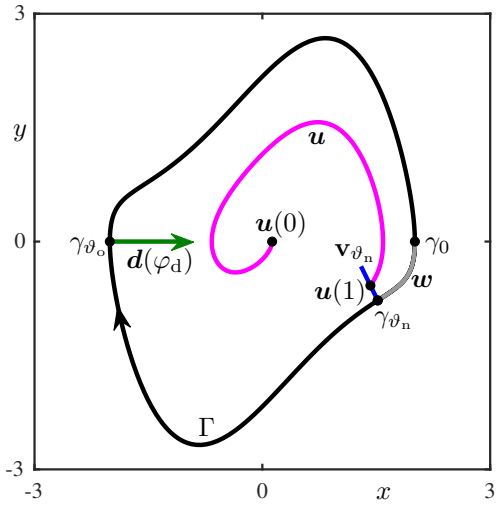

Figure 22: Schematic of the BVP setup with the periodic orbit Γ (black) of the Van der Pol system (14) with $\mu = 1$, showing the orbit segment $\boldsymbol{u}$ (magenta) with begin point $\boldsymbol{u}(1) = \gamma_{\vartheta_o} + A\,\boldsymbol{d}(\varphi_d)$ (here for $\vartheta_o = 0.5$, $\varphi_d = 0$ and $A \approx 1.8871$) and end point $\boldsymbol{u}(1)$ on the stable vector $\mathbf{v}_{\vartheta_n}$ (blue) at γ_{ϑ_n} (here for $\vartheta_n = 0.15$), and the orbit segment $\boldsymbol{w}$ (grey) with $\boldsymbol{w}(0) = \gamma_0$ and $\boldsymbol{w}(1) = \gamma_{\vartheta_n}$.

Acknowledgments

We thank Peter Langfield for helpful discussions.

A BVP setup for computing resetting surfaces

Winfree constructed system (7) in such a way that the isochrons are known as parametrised curves given by (6). As we explained, this yields implicitly defined expressions for the PTCs, the DTCs and the phase resetting surface graph($\mathcal{P}$), which we used to compute and render these objects.

However, it is not possible to derive formulas for the isochrons of a general vector field, such as the Van der Pol system (14). Hence, its isochrons, PTCs, DTCs and resetting surfaces of interest need to be computed numerically. To this end, we implemented the multi-segment boundary value problem (BVP) setup from [29] in the Matlab-based software package COCO [5], where we started from the demo files for computing isochrons in [19]. We present, here, for completeness a high-level explanation of the overall setup; the complete required boundary conditions can be found in [27, 28, 33] for computing isochrons, and in [19] for computing PTCs or DTCs. The computation of phase resetting curves can be performed for systems of any dimension, but we restrict here to the planar case where the direction vector $\boldsymbol{d}$ is given by the single angle $\varphi_d \in \mathbb{S}^1$.

The overall setup is sketched in Fig. 22 for the example of the Van der Pol system (14) with $\mu = 1$. Its central object is an orbit segment $\boldsymbol{u} = \{\boldsymbol{u}(s) \,|\, s \in [0,1]\}$ that satisfies the differential equation

$$\boldsymbol{u}' = K\,T_\Gamma\,\boldsymbol{F}(\boldsymbol{u}), \tag{17}$$

where time is rescaled by an integer multiple $K \in \mathbb{N}$ of the period T_Γ of Γ. At the begin and end points of $\boldsymbol{u}$ we impose the boundary conditions

$$\begin{aligned} \boldsymbol{u}(0) &= \gamma_{\vartheta_o} + A\,\boldsymbol{d}(\varphi_d) = \gamma_{\vartheta_o} + A\,[\cos(\varphi_d), \sin(\varphi_d)], && (18)\\ \boldsymbol{u}(1) &= \gamma_{\vartheta_n} + \eta\,\mathbf{v}_{\vartheta_n}. && (19) \end{aligned}$$

Here, $\mathbf{v}_{\vartheta_\mathrm{n}}$ is the stable unit eigenvector at the point $\gamma_{\vartheta_\mathrm{n}} \in \Gamma$ and $\eta \in \mathbb{R}$ is small. For this setup, it is assumed that we know $\gamma_{\vartheta_\mathrm{o}}$ for any $\vartheta_\mathrm{o} \in \mathbb{S}^1$, as well as $\gamma_{\vartheta_\mathrm{n}}$ and $\mathbf{v}_{\vartheta_\mathrm{n}}$ for any $\vartheta_\mathrm{n} \in \mathbb{S}^1$. In practice, this is achieved as follows. The periodic orbit Γ with its period T_Γ and its stable Floquet bundle are computed with a separate and quite standard BVP formulation with begin and end points at γ_0; for the latter, we use the formulation from [19, 33] with the adjoint variational equation. Moreover, an auxiliary orbit segment $\boldsymbol{w}$ with $\boldsymbol{w}(0) = \gamma_0$ and $\boldsymbol{w}(1) = \gamma_{\vartheta_\mathrm{n}}$ (and associated integration time), shown as the grey segment in Fig. 22, implements a 'shift' along Γ by ϑ_n and, hence, determines $\gamma_{\vartheta_\mathrm{n}}$ and $\mathbf{v}_{\vartheta_\mathrm{n}}$; see [29] for the details.

The key idea is that the orbit segment $\boldsymbol{u}$ with the boundary conditions (18) and (19) implements the defining property (3) with $\boldsymbol{d} = \boldsymbol{d}(\varphi_\mathrm{d})$ of the resetting function $\mathcal{P}$. Namely, for sufficiently small η, the point $\boldsymbol{u}(1)$ lies on I_{ϑ_n} to good approximation and, therefore, so does $\boldsymbol{u}(0)$ since it maps to $\boldsymbol{u}(1)$ under K iterations of the time T_Γ-map according to (17). We stress that this BVP formulation is very flexible. First of all, by selecting η as the continuation parameter that varies over an approximate fundamental domain near $\gamma_{\vartheta_\mathrm{n}}$ one can compute the isochron I_{ϑ_n} for given $\vartheta_\mathrm{n} \in \mathbb{S}^1$; see [19, 27, 33]. For the computation of resetting curves, there is complete freedom to choose either ϑ_o, φ_d or A as continuation parameter, while keeping the other two at fixed values of interest. Importantly, one can switch between different types of computations by changing which of these parameters is varied during a continuation. More specifically, fixing φ_d and A and varying ϑ_o gives the corresponding PTC as $\vartheta_\mathrm{n}(\vartheta_\mathrm{o})$ and, likewise, fixing ϑ_o and A and varying φ_d gives the corresponding DTC as $\vartheta_\mathrm{n}(\varphi_\mathrm{d})$. By appropriately switching between these two options, we compute a set of PTCs for a sequence of φ_d-values and/or a set of DTCs for a sequence of ϑ_o-values. Either of these sets of curves are then uses to render $\mathrm{graph}(\mathcal{P}_A)$ as a surface; to this end, we generate a suitable mesh from the curve data in the spirit of [20]. Changing to a continuation in A allows us to generate start data for any chosen value of A. A slice of $\mathrm{graph}(\mathcal{P})$ for fixed ϑ_o is computed from a set of DTCs in an analoguous way.

The respective one-parameter family of solutions of the overall multi-segement BVP is found in COCO by its orthogonal collocation BVP solver in conjunction with pseudo-arclength continuation. Notice that for $\vartheta_\mathrm{o} = \varphi_\mathrm{d} = A = 0$ the orbit segment representing Γ is a solution of (18) and (19) with $\eta = 0$ and for any K; hence, this special case can be used to start a continuation run. The advantage of implementing this in the software package COCO is that the number of mesh intervals for the discretisation of each segment can be chosen separately [5]. This is particularly useful here, because the orbit segment $\boldsymbol{u}$ is typically very long, compared with $\boldsymbol{w}$ and the orbit segments that represent Γ and its Floquet bundle.

References

[1] V. I. Arnold, *Singularity Theory*, Cambridge University Press, 2013.

[2] E. Brown, J. Moehlis and P. Holmes, On the phase reduction and response dynamics of neural oscillator populations, *Neural Comput.*, **16**(4) (2004) 673–715.

[3] O. Castejón and A. Guillamon, Phase-amplitude dynamics in terms of extended response functions: Invariant curves and Arnold tongues, *Commun. Nonlinear Sci. Numer. Simul.*, **81** (2020) 105008.

[4] O. Castejón, A. Guillamon and G. Huguet, Phase-amplitude response functions for transient-state stimuli. *J. Math. Neurosci.*, **3**(1) (2013) 1–26.

[5] H. Dankowicz and F. Schilder. *Recipes for Continuation.* SIAM, Philadelphia PA, 2013.

[6] M. Demazure, *Bifurcations and Catastrophes: Geometry of Solutions to Nonlinear Problems*, Springer Berlin Heidelberg, 2000.

[7] E. J. Doedel, AUTO, a program for the automatic bifurcation analysis of autonomous systems, *Congr. Numer.*, **30** (1981) 265–384.

[8] E. J. Doedel, AUTO-07P: Continuation and bifurcation software for ordinary differential equations, with major contributions from A.R. Champneys, T. F. Fairgrieve, Yu. A. Kuznetsov, B. E. Oldeman, R. C. Paffenroth, B. Sandstede, X. J. Wang and C. Zhang, Concordia University, 2007; available at `http://cmvl.cs.concordia.ca/auto/`

[9] E. J. Doedel, B. W. Kooi, G. A. K. van Voorn and Yu. A. Kuznetsov, Continuation of connecting orbits in 3D-ODEs (i): Point-to-cycle connections, *Int. J. Bifurcat. Chaos*, **18**(7) (2008) 1889–1903.

[10] J. L. A. Dubbeldam, J. L. A. and B. Krauskopf, Self-pulsations of lasers with saturable absorber: dynamics and bifurcations, *Opt. Commun.* **159**(4) (1999) 325–338.

[11] G. B. Ermentrout, Type I membranes, phase resetting curves, and synchrony. *Neural Comput.*, **8**(5) (1996) 979–1001.

[12] G. B. Ermentrout and D. H. Terman, *Mathematical Foundations of Neuroscience,* Interdisciplinary Applied Mathematics **35**, Springer-Verlag, Berlin Heidelberg, 2010.

[13] G. B. Ermentrout, L. Glass and B. E. Oldeman, The shape of phase-resetting curves in oscillators with a saddle node on an invariant circle bifurcation. *Neural Comput.*, **24**(12) (2012) 3111–3125.

[14] R. F. Galán, G. B. Ermentrout and N. N. Urban, Efficient estimation of phase-resetting curves in real neurons and its significance for neural-network modeling, *Phys. Rev. Lett.*, **94**(15) (2005) 158101.

[15] L. Glass and A. T. Winfree, Discontinuities in phase-resetting experiments, *Am. J. Physiol. Regul. Integr. Comp. Physiol.*, **246**(2) (1984) R251–R258

[16] J. Guckenheimer, Isochrons and phaseless sets, *J. Math. Biol.*, **1**(3) (1975) 259–273.

[17] A. Guillamon and G. Huguet, A computational and geometric approach to phase resetting curves and surfaces, *SIAM J. Appl. Dyn. Syst.*, **8**(3) (2009) 1005–1042.

[18] J. Hannam, B. Krauskopf and H. M. Osinga, Global isochrons of a planar system near a phaseless set with saddle equilibria, *The European Physical Journal – Special Topics*, **225**(13) (2016) 2645–2654.

[19] J. Hannam, B. Krauskopf and H. M. Osinga, Isochron foliations and global bifurcations: a case study, *Trans. Math. Appl.*, **6**(2) (2022) tnac002.

[20] J. Hannam, B. Krauskopf and H. M. Osinga, Global manifolds of saddle periodic orbits parametrised by isochrons, in S. Olaru, S. Elaydi, J. Cushing, and R. Lozi (Eds.), *Advances in Discrete Dynamical Systems, Difference Equations, and Applications*, Springer-Verlag, 2024, pp 143-174

[21] D. Hansel, G. Mato and C. Meunier, Synchrony in excitatory neural networks, *Neural Comput.*, **7**(2) (1995) 307–337.

[22] A. L. Hodgkin, The local electric changes associated with repetitive action in a non-modulated axon, *J. Physiol.*, **107**(2) (1948) 165–181.

[23] G. Huguet and R. de la Llave, Computation of limit cycles and their isochrons: Fast algorithms and their convergence, *SIAM J. Appl. Dyn. Syst.*, **12**(4) (2013) 1763–1802.

[24] M. Kawato and R. Suzuki, Biological oscillators can be stopped—Topological study of a phase response curve, *Biol. Cybern.*, **30**(4) (1978) 241–248.

[25] S. B. S. Khalsa, M. E. Jewett, C. Cajochen and C. A. Czeisler, A phase response curve to single bright light pulses in human subjects, *J. Physiol.*, **549**(3) (2003) 945–952.

[26] B. Krauskopf and H. M. Osinga, Computing invariant manifolds via the continuation of orbit segments; *Numerical Continuation Methods for Dynamical Systems* (eds. B. Krauskopf, H. M. Osinga and J. Galán-Vioque), Springer Berlin Heidelberg, 2007, 117–154.

[27] P. Langfield, B. Krauskopf and H. M. Osinga, Solving Winfree's puzzle: the isochrons in the FitzHugh–Nagumo model, *Chaos*, **24**(1) (2014) 013131.

[28] P. Langfield, B. Krauskopf and H. M. Osinga, Forward-time and backward-time isochrons and their interactions, *SIAM J. Appl. Dyn. Syst.*, **14**(3) (2015) 1418–1453.

[29] P. Langfield, B. Krauskopf and H. M. Osinga, A continuation approach to computing phase resetting curves. *Advances in Dynamics, Optimization and Computation* (eds. O. Junge, O. Schütze, G. Froyland S. Ober-Blobaum and K. Padberg-Gehle), Springer-Verlag, New York, 2020, 3–30.

[30] B. Monga, D. Wilson, T. Matchen and J. Moehlis, Phase reduction and phase-based optimal control for biological systems: A tutorial. *Biol. Cybern.*, **113**(1–2) (2019) 11–46.

[31] H. Nakao, Phase reduction approach to synchronisation of nonlinear oscillators, *Contemp. Phys.*, **57**(2) (2016) 188–214.

[32] A. N. Nicholson, M.B. Spencer, P. A. Pascoe, B. M. Stone, T. Roehrs and T. Roth, Sleep after transmeridian flights, *Lancet*, **328**(8517) (1986) 1205–1208.

[33] H. M. Osinga and J. Moehlis, Continuation-based computation of global isochrons, *SIAM J. Appl. Dyn. Syst.*, **9**(4) (2010) 1201–1228.

[34] J. Palis and W. de Melo, *Geometric Theory of Dynamical Systems*, Springer-Verlag, New York, 1982.

[35] T. Poston and I. Stewart, *Catastrophe Theory and its Applications*, Dover Publications, Mineola, N.Y, 1996.

[36] K. Ota, M. Nomura and T. Aoyagi, Weighted spike-triggered average of a fluctuating stimulus yielding the phase response curve, *Phys. Rev. Lett.*, **103**(2) (2009) 024101.

[37] K. Ota, T. Omori, S. Watanabe, H. Miyakawa, M. Okada and T. Aonishi, Measurement of infinitesimal phase response curves from noisy real neurons, *Phys. Rev. E*, **84**(4) (2011) 041902.

[38] A. Pérez-Cervera, T. M. Seara and G. Huguet, A geometric approach to phase response curves and its numerical computation through the parameterization method, *J. Nonlinear Sci.*, **29**(6) (2019) 2877–2910.

[39] B. Pietras and A. Daffertshofer, Network dynamics of coupled oscillators and phase reduction techniques, *Phys. Rep.*, **819** (2019) 1–150.

[40] N.W. Schultheiss, A.A. Prinz and R.J. Butera (Eds.), *Phase Response Curves in Neuroscience: Theory, Experiment, and Analysis*, (NEUROSCI, volume 6) Springer-Verlag, Cambridge MA, 2012.

[41] T. Tateno and H. P. C. Robinson, Phase resetting curves and oscillatory stability in interneurons of rat somatosensory cortex, *Biophys. J.*, **92**(2) (2007) 683–695.

[42] B. van der Pol, A theory of the amplitude of free and forced triode vibrations, *Radio Rev.*, **1** (1920) 701–710.

[43] B. van der Pol, On relaxation oscillations, *Lond. Edinb. Dublin Philos. Mag. J. Sci.* , **2**(11) (1926) 978–992.

[44] B. van der Pol, The nonlinear theory of electric oscillations, *Proc. Inst. Radio Eng.*, **22**(9) (1934) 1051–1086.

[45] J. Waterhouse, T. Reilly, G. Atkinson and B. Edwards, Jet lag: trends and coping strategies, *Lancet*, 369(9567) (2007) 1117–1129.

[46] K. C. A. Wedgwood, K. K. Lin, R. Thul and S. Coombes, Phase-amplitude descriptions of neural oscillator models, *J. Math. Neurosci.*, **3** (2013) 2.

[47] A. T. Winfree, Time and Timelessness in Biological Clocks, in J Urquhart, F. E. Yates (eds), *Temporal Aspects of Therapeutics*, ALZA Conference Series, vol 2, Springer, Boston, MA, 1973, pp 35–49.

[48] A. T. Winfree, Patterns of phase compromise in biological cycles, *J. Math. Biol.* **1**(1) (1974) 73–93.

[49] A. T. Winfree, *The Geometry of Biological Time*, 2nd ed., Springer-Verlag, New York, 2001.

[50] M. Yamada, A theoretical analysis of self-sustained pulsation phenomena in narrow stripe semiconductor lasers, *IEEE J. Quantum Electron.* **29** (1993) 1330.